Elsevier Editorial System(tm) for Chemical Geology
Manuscript Draft

Manuscript Number: CHEMGE7149R1

Title: Mesoarchaean aluminous rocks at Storø, southern West Greenland: new age data and evidence of premetamorphic seafloor weathering of basalts

Article Type: Research Article

Keywords: Archaean; Greenland; Supracrustal belt; Storø; Premetamorphic alteration; Seafloor weathering

Corresponding Author: Mr. Kristoffer Szilas, Ph.D.

Corresponding Author's Institution: Lamont-Doherty Earth Observatory

First Author: Kristoffer Szilas, Ph.D.

Order of Authors: Kristoffer Szilas, Ph.D.; Adam A Garde, Ph.D.

Abstract: Metamorphosed Meso- to Neoarchaean supracrustal rocks in the central part of the island of Storø (Nuuk region, southern West Greenland), show field- and geochemical evidence of premetamorphic chemical alteration. This alteration changed basaltic precursors into aluminous lithologies, and following amphibolite grade metamorphism and penetrative ductile deformation, these garnet-biotite schists now resemble adjacent metapelitic schists of sedimentary origin. Mass balance calculations (isocon method), suggests that most major elements (Si, Fe, Mg, Ca, Na and P) were leached during alteration. The calculated overall net mass changes are between -18% and -45%, consistent with breakdown of olivine, pyroxenes, plagioclase and apatite in the basaltic precursor rocks. Major and trace elements such as, K, Cs, Rb, Ba, Pb, Zn, La, Ce were added during this alteration process, whereas high field strength elements (Ti, Al, Zr, Hf and Nb) remained essentially immobile and were thus residually enriched. Interestingly, Th which is generally assumed to be immobile in fluids, was also added during this process. These chemical changes reflect interaction between a basaltic protolith and hydrous fluids that established a new equilibrium and thus a different mineral assemblage. It is proposed that the premetamorphic alteration at Storø was due to low-temperature interaction between seawater and oceanic crust, and thus essentially represents in situ submarine seafloor weathering. This interpretation is consistent with the mass balances reported from well-documented examples in younger settings.
New U-Pb zircon geochronology from the arc-related mafic sequences at Storø shows that they comprise at least two distinct age groups: an older anorthosite complex dated at 3051.3 ± 2.6 Ma and a younger supracrustal sequence with age brackets between 2840-2710 Ma. The allochthonous nature of these two mafic igneous to sedimentary stacks is consistent with accretionary processes in island arc complexes and a compressional Archaean tectonic setting.

Graphical Abstract (for review)

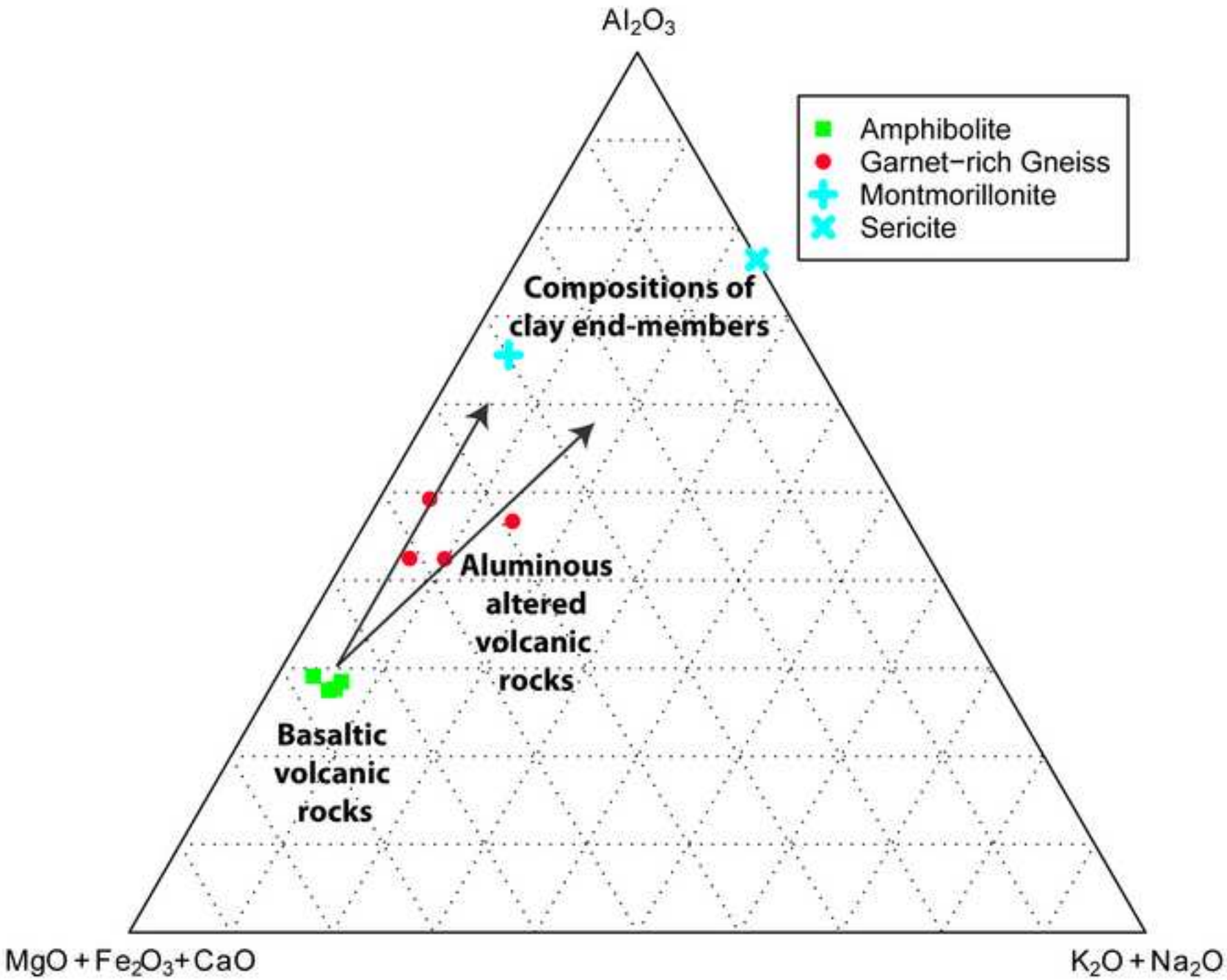

***Highlights (for review)**

- Garnet-rich gneisses on Storø have similar immobile element ratios as amphibolites.
- These garnet-rich gneisses were derived from basalts by premetamorphic alteration.
- Isocon mass-balance calculations show similarities to modern seafloor weathering.

Mesoarchaean aluminous rocks at Storø, southern West Greenland: new age data and evidence of premetamorphic seafloor weathering of basalts

Kristoffer Szilas [a, b, *], Adam A. Garde [a]

[a] Geological Survey of Denmark and Greenland, Øster Voldgade 10, 1350, Copenhagen, Denmark

[b] Lamont-Doherty Earth Observatory, PO Box 1000, Palisades, NY 10964-8000, USA

* Corresponding author at: Lamont-Doherty Earth Observatory, PO Box 1000, Palisades, NY 10964-8000, USA

Corresponding author e-mail: kszilas@ldeo.columbia.edu

Abstract

Metamorphosed Meso- to Neoarchaean supracrustal rocks in the central part of the island of Storø (Nuuk region, southern West Greenland), show field- and geochemical evidence of premetamorphic chemical alteration. This alteration changed basaltic precursors into aluminous lithologies, and following amphibolite grade metamorphism and penetrative ductile deformation, these garnet-biotite schists now resemble adjacent metapelitic schists of sedimentary origin. Mass balance calculations (isocon method), suggests that most major elements (Si, Fe, Mg, Ca, Na and P) were leached during alteration. The calculated overall net mass changes are between -18% and -45%, consistent with breakdown of olivine, pyroxenes, plagioclase and apatite in the basaltic precursor rocks. Major and trace elements such as, K, Cs, Rb, Ba, Pb, Zn, La, Ce were added during this alteration process, whereas high field strength elements (Ti, Al, Zr, Hf and Nb) remained essentially immobile and were thus residually enriched. Interestingly, Th which is generally assumed to be immobile in fluids, was also added during this process. These chemical changes reflect interaction between a basaltic protolith and hydrous fluids that established a new equilibrium and thus a

different mineral assemblage. It is proposed that the premetamorphic alteration at Storø was due to low-temperature interaction between seawater and oceanic crust, and thus essentially represents *in situ* submarine seafloor weathering. This interpretation is consistent with the mass balances reported from well-documented examples in younger settings.

New U-Pb zircon geochronology from the arc-related mafic sequences at Storø shows that they comprise at least two distinct age groups: an older anorthosite complex dated at 3051.3 ± 2.6 Ma and a younger supracrustal sequence with age brackets between 2840–2710 Ma. The allochthonous nature of these two mafic igneous to sedimentary stacks is consistent with accretionary processes in island arc complexes and a compressional Archaean tectonic setting.

Keywords: Archaean; Greenland; Supracrustal belt; Storø; Premetamorphic alteration; Seafloor weathering

1. Introduction

Metavolcanic belts in Archaean cratons constitute a major source of Au and other metals worldwide (Goldfarb et al., 2001). The origin of the supracrustal host rocks and their common Au deposits have been much debated, especially in polymetamorphosed and deformed rocks where the protoliths are not easily recognisable (e.g. Groves et al., 2003). For instance, the metavolcanic rocks are commonly associated with garnet-rich aluminous schists that superficially appear to be of sedimentary origin, but which lack lithological layering akin to transposed bedding.

Both epithermal, orogenic and volcanogenic-massive-sulfide mineralisation processes are well understood and closely associated with specific types of hydrothermal alteration and controlled by host rock compositions and fabrics including porosity and permeability, as well as heat and fluid

sources, ambient temperature and hydrostatic pressure gradients (Hedenquist and Lowenstein, 1994; Eilu and Groves, 2001; Herrington et al., 2005). Various low-temperature subaqueous and subaerial weathering processes can also lead to significant chemical alteration (e.g. Alt and Teagle, 2003; Polat et al., 2012). Due to this difficulty in identifying different alteration processes through metamorphic overprint, several orogenic deposits have for example now been reinterpreted as metamorphosed epithermal (and in a few cases volcanogenic-massive-sulfide) deposits (Hallberg, 1993; Penczak and Mason, 1999; Bonnet et al., 2005; McFarlane et al., 2007; Owens and Pasek, 2007; Garde et al., 2012). Such distinctions are important not least for future Au exploration.

Identifying different types of alteration in highly deformed and metamorphosed rocks can be challenging, because the bulk composition of leached rocks may be similar to that of rocks derived by sedimentary processes. Archaean aluminous schists and gneisses within supracrustal belts in the North Atlantic craton of southern West Greenland have therefore been interpreted as metasedimentary rocks (e.g. Rivalenti and Rossi, 1972), as various kinds of chemically altered (meta)volcanic rocks (e.g. Beech and Chadwick, 1980; Dymek and Smith, 1990; Garde et al., 2007, 2012), or as a combination of both (Smith et al., 1992; Bolhar et al., 2005).

In this paper we describe and discuss the nature of chemical alteration of Archaean arc-related mafic metavolcanic rocks on the island of Storø in Godthåbsfjord, in the central North Atlantic craton of southern West Greenland. It is shown that a conspicuous component of aluminous rocks, which superficially resembles adjacent metasedimentary rocks, likely formed during the interaction between mafic rocks and cold seawater, implying that the combined sequence of mafic metavolcanic and aluminous lithologies are likely to represent a section through Archaean oceanic crust.

We also present new geochronological data, which corroborate that the central part of Storø comprises at least three different tectonic slices of Eoarchaean to Neoarchaean crust including at

least two different age groups of mafic rock sequences that were juxtaposed during Neoarchaean tectonic amalgamation of older magmatic arcs (e.g. Nutman and Friend, 2007).

2. Geological setting

The island of Storø is located in the central part of the largely Mesoarchaean North Atlantic craton that forms most of southern Greenland and continues as the Nain Province in eastern Labrador (**Fig. 1**; Schiøtte et al., 1989; Schiøtte and Bridgwater, 1990; St-Onge et al., 2009). In southern West Greenland the craton has recently been divided into six tilted crustal blocks that expose the root zones of several convergent andesitic island arc – continental arc systems and oceanic supra-subduction zones (Garde, 2007; Polat et al., 2007; Windley and Garde, 2009; Szilas et al., 2012, 2013a, 2013b). Storø itself is located at the south-eastern margin of the >3000 Ma Fiskefjord block of Windley and Garde (2009), previously referred to as the Akia terrane (e.g. Friend et al., 1996). The complex, collisional Godthåbsfjord–Ameralik belt to its south-east, which also comprises the eastern part of Storø, consists of several smaller terranes of different origin and age that were tectonically assembled and folded at around 2720 Ma (Friend et al., 1996). Following the assembly of the Fiskefjord block and the terranes to the south-east, Storø and adjacent parts of the Godthåbsfjord–Ameralik belt were intruded by c. 2650–2550 Ma granitoid crustal melts including the 2550 Ma Qôrqut granite complex (Brown et al. 1981; Friend et al. 1996; Nutman and Friend, 2007; Nutman et al., 2007, 2010). This resulted in an extensive network of granitic pegmatites throughout the supracrustal rocks in central Storø.

The central part of Storø consists of a stack of supracrustal rocks of different age and composition that have been referred to as the 'Storø supracrustal belt' or 'Storø greenstone belt' in the literature, most recently by Scherstén et al. (2012). Existing age data quoted below are from

Scherstén et al. (2012) and stem from GEUS reports cited therein. The supracrustal rocks constitute a major, in part refolded anticlinal structure with a NNW–SSE-trending hinge zone on the mutually facing slopes of the Qingaaq and Aappalaartoq mountains (**Fig. 2**) and are cut by an inclined, Neoarchaean shear zone along the north-western side of the island. The northern part of the stacked supracrustal and associated metagabbroic and anorthositic rocks on Aappalaartoq have been intruded by Mesoarchaean tonalitic orthogneiss. The south-eastern side of the stack is in presumed tectonic contact with Eoarchaean orthogneiss (previously termed Amîtsoq gneisses, now recognised as part of the Itsaq gneiss complex; Nutman et al., 1996). The supracrustal stack includes (1) metavolcanic tholeiitic amphibolite with island-arc geochemical signature yielding a metamorphic U-Pb zircon age of c. 2630 Ma but with a currently unknown protolith age, (2) undated garnet-rich, biotite- and sillimanite-bearing rocks that have previously been interpreted as either sedimentary or altered metavolcanic rocks, and (3) metasedimentary mica schist and biotite gneiss with detrital zircon grains yielding ages of ~2840 Ma, as well as both older and younger metamorphic grains (van Gool et al., 2007). This supracrustal stack is in tectonic contact with (4) remnants of a metagabbro–anorthosite complex intruded by c. 3050 Ma tonalitic orthogneiss.

The supracrustal rocks on Storø host a large, subeconomic Au occurrence that has been investigated in detail since the 1990s by surface mapping, geochemical and isotopic studies, drilling and 3D modelling (Grahl-Madsen, 1994; Trepka-Bloch, 1996; Skyseth, 1996; Appel et al., 2003; Hollis, 2005; Scherstén et al., 2012). The occurrence of Au in the supracrustal rocks at central Storø has been investigated in detail in recent years by the exploration company NunaMinerals A/S. Gold mainly occurs in two zones on the north-east-facing slope of the mountain of Qingaaq (**Fig. 2**; Østergaard and van Gool, 2007; Scherstén et al., 2012). The first, 'BD zone' is strata bound within the above mentioned garnet-rich rocks. The second, 'Main zone' is located in the hinge zone of a nearby Neoarchaean anticlinal fold, where the Au is mainly confined to late quartz veins

(Østergaard and van Gool, 2007). The latter authors proposed a structural model that links formation of the anticline with the above mentioned Neoarchaean shear zone flanking the supracrustal stack. Their model is supported by Re-Os age data from arsenopyrite, which yielded different ages for the two zones, suggesting that Au was introduced into the BD zone at c. 2710 Ma and partly remobilised into the 'Main zone' at c. 2630 Ma (Scherstén et al., 2012). Nutman et al. (2007) also obtained the latter age from U-Pb ion probe geochronology of zircon associated with sulphides in the 'Main zone' and argued that this represents the main Au mineralisation event.

The new Re-Os age data overrule a previously proposed age of ~2863 Ma for the Au mineralisation (Juul-Pedersen et al. 2007), which was based on Pb-Pb isotope data. The latter age likely represents the deposition of the younger volcanic-sedimentary supracrustal sequence on Storø, in agreement with the maximum deposition age of c. 2840 Ma for the metasedimentary rocks reported by van Gool et al. (2007).

Garnet-biotite thermobarometry of the supracrustal rocks on Storø has yielded (minimum) peak metamorphic temperatures of 521-624°C and pressures of 4.5–6.1 kbar (Hollis, 2005; Persson, 2007). This metamorphic event took place at c. 2630 Ma, based on U-Pb data from zircon rims (Hollis, 2005; Nutman et al., 2007).

3. Field relationships and petrography

Detailed observations from a traverse across the Au-hosting 'BD zone' and its wall rocks in the central part of the supracrustal stack on the Qingaaq mountain in central Storø between localities 79 and 83 are presented here (**Fig. 2)**. These localities are located in the west-facing slope of 'Lille Qingaaq' below the main mountain top, which can be traversed by foot. The geochemical compositions and element variations in ten samples along the traverse are presented and discussed

146 in subsequent sections. The samples are grouped into the following units from top to bottom: (1)
147 fragmental to massive amphibolite, (2) garnet-rich gneiss, (3) biotite gneiss and (4) layered
148 amphibolite.

149 The traverse begins in fragmental to massive mafic amphibolite in the hanging wall, moves into
150 garnet-rich gneiss of the 'BD zone', crosses the biotite-rich gneiss from which we present new
151 detrital zircon U-Pb age data, and ends in layered amphibolite of variable, mafic to intermediate
152 composition. The latter rocks contain dacitic layers for which we also present new U-Pb age data.
153 The lithological units as employed here are essentially the same as those used in central Storø by
154 van Gool et al. (2007).

155 The hanging wall amphibolite (unit 1) of the traverse consists of a dark, fine- to medium grained,
156 homogeneous to locally layered, and in places fragmental rock mainly composed of hornblende and
157 plagioclase and up to 10% titanite (**Fig. 3a-b**). The metamorphic textures appear well-equilibrated.
158 We interpret these rocks mainly as mafic lava flows, although evidence for a pyroclastic origin has
159 also been documented for rocks from one locality (van Gool et al., 2007). The analysed samples
160 (477610–12) are fresh, homogeneous, fine- to medium-grained hornblende-plagioclase-titanite
161 bearing rocks. Small proportions of garnet and biotite are commonly also observed, especially near
162 the contact with unit 2. Amphibolite sample 477613 at the contact with the garnet-rich gneiss (unit
163 2) contains a few per cent almandine garnet.

164 The garnet-rich gneiss of unit 2 is 1–4 m thick and displays a characteristic, highly variable but
165 diffuse layering. Its contact with the hanging wall amphibolite appears knife-sharp in the field (**Fig.**
166 **3b**). The rock has a granular texture. Garnet is mostly evenly distributed within each layer and
167 contains inclusions of staurolite. Foliation is weak or absent, but the crude layering is folded into
168 irregular, open to tight, decimetre-scale folds.

The lithological layering and predominant aluminous mineralogy of unit 2 have previously led to the interpretation that these rocks represented metamorphosed pelitic schists of clastic sedimentary origin (Pedersen, 1996; Persson, 2007). However, these rocks do not display any distinct schistosity and do not contain any anatectic granitic veins, unlike genuine metaclaystone or metagreywacke where anatectic veins would be common and widespread at this metamorphic grade. The rocks of unit 2 possess a non-sedimentary aluminous composition that prevents upper amphibolite facies partial melting.

Darker parts of the garnet-rich gneiss reveal rounded to elongate, and in some places folded pods and layers of mafic amphibolite about 10–20 cm thick, which contain small proportions of evenly distributed garnet, and gradational boundaries into the predominant garnet-rich, amphibole-absent lithologies (**Fig. 3c-d**). These observations suggest that (1) the garnet-rich gneiss has been derived by chemical alteration of a mafic volcanic precursor, and (2) the alteration took place prior to metamorphism and folding. It has previously been proposed, based on their geochemistry, that such rocks in central Storø represent alteration products (Eilu et al., 2006; Knudsen et al., 2007; Szilas, 2008).

The biotite gneiss of unit 3 is well-foliated, compositionally layered and fine to medium grained, and comprises biotite, quartz, plagioclase, sillimanite and minor garnet. The biotite gneiss (**Fig. 3e-f**) displays gradational compositional layering with sharp internal boundaries suggestive of flattened, transposed and recrystallised graded bedding. Pods and stringers of quartz are common and interpreted as relict premetamorphic quartz veins. Migmatitic melt seams are abundant, as would be expected during high grade metamorphism of claystone. A sedimentary origin is corroborated by a detrital zircon population in sample 477609, with new age data presented below (**section 5.2**). The contact to the hanging wall garnet-rich gneiss is sharp, but it is difficult to determine if it is primary or tectonic. The biotite gneiss may be equivalent to the biotite (-garnet)

gneiss sample 487416 collected approximately 500 m to the north-east (still on the western slope of 'Lille Qingaaq'), which was described by van Gool et al. (2007).

Layered amphibolite (unit 4) forms the footwall sequence below the biotite gneiss (unit 3), with a possible or likely tectonic contact. This unit mainly consists of strongly deformed, grey, biotite-bearing amphibolite which occasionally displays a uniform, millimetre- to centimetre-scale layering (**Fig. 3g**). The rocks of unit 4 have a mafic to dacitic composition (van Gool et al. 2007) and are interpreted by us as deformed and metamorphosed pyroclastic deposits. A deformed, medium-grained, felsic layer (25 cm thick) within this unit was sampled for age determination (**Fig. 3h**; sample 477618), see **section 5.2**. Due to intense deformation and apparent concordance with the adjacent rocks it is difficult to determine if this sheet is a metamorphosed felsic tuff or an intrusive granitoid rock. We interpret the entire unit 4 as pyroclastic in origin, however this has no bearing on the interpretation of the age data from the felsic layer presented in section 5.2.

Granitic sheets and pegmatites related to the 2550 Ma Qôrqut Granite Complex form an extensive network throughout all supracrustal rocks in central Storø (Fig. 2).

4. Analytical methods

4.1. Whole rock major and trace element analysis

Major element geochemical data were acquired by X-ray fluorescence (XRF) at the Geological Survey of Denmark and Greenland (GEUS). The data are presented in **Table 1** in the online supplementary material. See Kystol and Larsen (1999) for a detailed description of the analytical procedures.

Trace element data were obtained by inductively coupled plasma mass-spectrometry (ICP-MS) methods likewise at GEUS, using the fused borate discs from the XRF analysis. The use of the borate disc for trace element analysis ensures complete dissolution of all mineral phases but at the expense of analytical precision. However, the verification (supplementary data, Table 1, including 32 runs of the Disko-1 standard) shows that the Storø data set is sufficiently accurate and precise for their present purpose.

The trace element procedure is as follows: 0.5–1.0 g of the borate disc used for XRF-analysis is dissolved by nitric and hydrofluoric acid. The open Savillex vessel is placed on a hotplate at 180° C until the acids have evaporated. Nitric acid is then added and evaporated to dryness in two cycles. Nitric acid, internal standard solution (Ge, Rh, Re) and water are added. The vessel is closed and placed on a hotplate at 130° C for at least 12 hours. The sample is then diluted to 50 ml and just before measurement the sample is diluted further 11 times. For calibration of the instrument, certified solutions containing REE's and some additional elements are used. For verification an in-house standard (Disko-1), three international reference samples (BE-N, GA and GH), two blanks and one borate blank are prepared at the same time as the samples. The trace elements are measured using a PerkinElmer Elan 6100DRC ICP-MS instrument. The set-up, data acquisition, calibration and calculations are done using the Elan software version 2.3.2.

4.2. Zircon U-Pb isotope analysis

Separated zircons were hand-picked, mounted in transparent epoxy together with a reference zircon, and polished sufficiently to reveal cores. Scanning electron microscope (SEM) backscatter and cathode luminescence images of the internal structure of the grains were made using a Philips instrument at GEUS. The U-Th-Pb analyses were performed using a single-collector, magnetic

sectorfield LA-ICP-MS instrument at GEUS (sample 477609) and with the Cameca ims1270 instrument at the Nordsim laboratory, Swedish Museum of Natural History (sample 477618). The analytical procedures for the LA-ICP-MS and ion probe work closely followed those described by Frei and Gerdes (2009) and Whitehouse et al. (1999) and Whitehouse and Kamber (2005), respectively, with the 1065 Ma Geostandards zircon 91500 used as a reference for calculating U/Pb ratios. Where the amount of 204Pb indicates the likely presence of common Pb, this was corrected using the present day terrestrial Pb composition of Stacey and Kramers (1975). Age regression was done using Isoplot of Ludwig (2003), with results presented at the 95% confidence level.

The U-Pb geochronological data are shown in **Fig. 7b-7c** and listed in **Table 2** of the supplementary data.

5. Analytical results

5.1. Whole-rock geochemical data

The same lithological groups as outlined in section 3, based on the field appearance and mineralogy, were employed in this section. The MFW weathering index of Ohta and Arai (2007) was used to identify which of the samples show signs of weathering and/or alteration relative to the igneous evolution trend. This is shown as the magnitude of the W index in **Figure 4**). The whole-rock geochemical composition is recalculated on a volatile-free basis and we use recalculated compositions throughout this paper. All diagrams are plotted using the software GCDkit of Janoušek et al. (2006).

The amphibolite samples (n=4) are basaltic with 48.6–49.8 wt.% SiO_2, 5.8–6.8 wt.% MgO and 1.7–1.9 wt.% TiO_2, and plot as Fe-tholeiites in various discrimination diagrams (e.g. Irvine and

Baragar, 1971; Jensen, 1976; Miyashiro, 1974). As seen in **Fig. 5**, their trace element patterns are relatively flat with no distinct anomalies in the elements that are generally fluid-immobile, except for a slight enrichment in Th and a small positive Zr anomaly relative to primitive mantle. Their chondrite-normalised (Boynton, 1984) La_{CN}/Sm_{CN} ratio is 0.78-0.89. The amphibolites have a W-index of 4.2-4.5 with one outlier (477613) at a W index of 9.1 and a Zr/TiO_2 ratio varying between 63 and74.

The garnet-rich gneisses (n=4) contain 49.6–53.2 wt.% SiO_2, 2.3–3.0 wt.% MgO and 1.80–2.75 wt.% TiO_2, and have fractionated REE with La_{CN}/Sm_{CN} of 1.48–2.11. They are distinctly peraluminous with 19.1–23.1 wt.% Al_2O_3. Their W index is 19.2–27.0. They have Zr/TiO_2 ratios of 66–78, with one outlier at 113 (sample 477607).

The analysed sample of biotite gneiss contains 70.8 wt.% SiO_2, 2.69 wt.% MgO and 0.71 wt.% TiO_2 and is peraluminous with 14.2 wt.% Al_2O_3 and a W index of 36. The sample has an enriched trace element pattern with La_{CN}/Sm_{CN} of 3.3, a distinctly negative Nb anomaly, a small negative Ti anomaly (**Fig. 5**) and a Zr/TiO_2 ratio of 154.

The analysed sample of layered amphibolite has 68.1 wt.% SiO_2, 1.05 wt.% MgO and 0.35 wt.% TiO_2 and is thus of dacitic composition, whereas the overall unit appears to be andesitic due to predominance of more mafic layers (**section 3**). Normalised to primitive mantle it has a distinctly enriched trace element pattern with a negative Nb anomaly, a large positive Zr anomaly (**Fig. 5**) and Zr/TiO_2 of 741. It has a La_{CN}/Sm_{CN} ratio of 6.1, which is distinctly different from the mafic amphibolites. Concentrations of compatible elements are low, with 6.9 ppm Ni and of 3.6 ppm Cr.

The geochemical profile from massive amphibolite through garnet-rich gneiss and into biotite gneiss shows that although the garnet-rich gneiss is distinctly peraluminous, its immobile element ratios are comparable to those of the amphibolite, as seen on plots of TiO_2, Nb, Lu and Hf versus Zr

(**Fig. 8**). However, one sample of garnet-rich gneiss (477607) has immobile element ratios that are intermediate between biotite gneiss and amphibolite.

5.2. U-Pb zircon geochronology

Sample 477618 from the layered amphibolite in the tectono-stratigraphically lowest part of the traverse contains stubby prismatic zircon grains with generally well-preserved oscillatory and sector zonation (**Fig. 7a**). Metamorphic overgrowths occur but are only a few microns thick, too narrow to be analysed. Eighteen out of 28 analysed grains yield a mean $^{207}Pb/^{206}Pb$ age of 3051.3 ± 2.6 Ma (2σ), MSWD = 3.7 (**Fig. 7b; Table 2** of electronic appendix), which is interpreted as a magmatic age. The dated population also comprises a couple of older (inherited?) grains, as well as a tail of younger grains yielding dates down to c. 2800 Ma (**Fig. 7b**). We interpret these as due to partial resetting during subsequent metamorphism (see discussion). The new age of 3051.3 ± 2.6 Ma demonstrates that the tectono-stratigraphically lowest part of the supracrustal rocks on Qingaaq (and presumably including the adjacent metagabbro and anorthosite) is contiguous with the lowest part of the mafic sequence on Aappalaartoq (**Fig. 2**; Hollis et al. 2005).

The detrital $^{207}Pb/^{206}Pb$ zircon age data from biotite gneiss sample 477609 are shown in **Fig. 7c** and **Table 2** of the online supplementary material. The age distribution is comparable to a previous data set from another metasedimentary rock that probably represents a tectono-stratigraphic equivalent (sample 484601; Scherstén et al., 2012) and corroborates that the central and possibly also upper part of the supracrustal sequence was deposited at or after 2840 Ma. Assuming that the biotite gneiss is *in situ* with respect to the chemically altered garnet-rich gneiss, this age is also the maximum age of the alteration and initial Au mineralisation.

6. Discussion

6.1. Whole-rock geochemical signatures

Three of the four amphibolite samples appear to represent isochemically metamorphosed basaltic rocks. Ordóñez-Calderón et al. (2011) showed that the amphibolites on Storø are generally tholeiitic basalts with island arc chemical affinity. Our amphibolite samples are similar to the 'upper amphibolites' presented in their study and confirm the island arc tholeiitic signature of these metavolcanic rocks. Sample 467613 has a W index of 9.1, which is slightly elevated relative to values of 4.2–4.5 for the essentially unaltered amphibolites. This sample also has slight enrichment in light rare earth elements (LREE) and K_2O. This is consistent with the observation that this particular sample is located at the contact to the garnet-rich gneiss unit and contains some garnet and biotite (**section 3**). Thus, the chemical boundary between the two units is not as sharp as it might appear in outcrop (Fig. 3b). This sample has likely been affected by element mobility during the alteration that affected the garnet-rich gneiss precursor (**section 6.2**).

The dacitic component of the layered amphibolite at locality 83 at the base of the traverse has a trace element pattern that is distinctly different from the mafic amphibolites of unit 1. The observed REE fractionation with a La_{CN}/Sm_{CN} ratio of 6.1 is too great to have been derived from melts represented by amphibolite unit 1 by fractional crystallisation. This is consistent with the older U-Pb zircon age of ~3050 Ma obtained from the layered amphibolite unit (**section 5.2**). The two amphibolite units therefore belong to juxtaposed igneous mafic and volcanosedimentary sequences of different origin.

The garnet-rich gneisses plot with a pelitic composition in sedimentary discrimination diagrams of Herron (1988; not shown), which is based on their major element compositions. Although the

garnet-rich gneiss and biotite gneiss units resemble each other mineralogically, they possess significant geochemical differences. In particular, the garnet-rich gneisses are enriched in high field strength elements (HFSE) and heavy rare earth elements (HREE). The fact that the HFSE and HREE ratios of the garnet-rich gneisses overlap with those of the tholeiitic amphibolites (**Fig. 8**) strongly supports the field evidence that the garnet-rich gneiss stems from a basaltic precursor (**section 3**). This is also seen from the total REE patterns, where the HREE are elevated in the residual alteration product relative to the basaltic precursor, whereas the LREE were apparently mobilised and become slightly fractionated and enriched. We also note that the biotite gneisses have similar Zr/Hf ratios as the amphibolites, which suggest a significant contribution from a mafic protolith to these metasedimentary rocks.

The new observations and geochemical data presented here corroborate previous suggestions that the garnet-rich gneiss represents an alteration product of a mafic volcanic precursor (Eilu et al., 2006; Knudsen et al., 2007; Szilas, 2008), although the specific type of alteration was not defined in these earlier studies.

It can be ruled out that the chemical alteration represents palaeosol formation on basalt, because of the remnants of unaltered amphibolite within the garnet-rich gneiss (**Fig. 3c-d**). In addition, the adjacent biotite gneiss is interpreted as sedimentary and likely to represent a subaqueous deposit. Additionally, the presence of amphibolite remnants also rule out the possibility that the garnet-rich gneiss represents erosion products derived from a mafic source. On the other hand, the garnet-rich gneiss could conceivably have been derived by subaqueous alteration of a basaltic precursor, either by low-temperature seafloor weathering prior to or during deposition of the metasedimentary biotite gneiss unit, or by subsequent infiltration of hydrothermal fluids along this lithological contact.

In the following section we focus on this alteration from amphibolite to garnet-rich gneiss and provide mass balance calculations for this process.

359

360 6.2. Isocon mass balance calculations

361

362 The hypothesis that the garnet-rich gneiss is an alteration product from the massive
363 amphibolite precursor can be tested with mass balance calculations, considering that the field
364 relationships indicate that the alteration occurred prior to metamorphism and assuming that only
365 minor and insignificant element changes occurred during the metamorphism. For this test we use
366 the isocon method of Grant (1986, 2005). This method relies on the fact that certain elements
367 remain immobile during alteration and define a so-called isocon line, which has a slope that is
368 proportional to the net mass change. The change can be quantified by comparing an altered sample
369 with its precursor (Gresens, 1967). The average composition of the three least altered amphibolites
370 (477610, 477611 and 477612) was chosen as a hypothetical precursor in order to minimise the
371 effects of possible crystal fractionation. It was assumed that TiO_2, Zr, Hf, Nb and Lu remained
372 essentially immobile during the alteration, which is supported by a high regression coefficient of the
373 isocon lines. The results of the isocon calculations are shown in **Fig. 9** and **Table 3** in the online
374 supplementary material. Even small discrepancies between the true precursor and the chosen
375 median value might affect the mass calculation. Such discrepancies could arise from fractional
376 crystallisation through the mafic sequence or addition of a possible detrital component, given the
377 presence of genuine sedimentary rocks within the supracrustal pile. Therefore the actual numerical
378 results are considered less significant than the qualitative information describing which elements
379 were mobilised on a broader scale.

380 As already noted, the amphibolite located immediately next to the alteration zone (sample
381 477613) contains some garnet and biotite. This sample has slightly elevated LREE and K_2O and
382 could thus represent a transitional stage to an alteration product such as the garnet-rich gneiss, in

agreement with the calculated mass changes. There is a systematic progression in the intensity of alteration from the slightly altered amphibolite (477613), which has a net mass loss of -18 %, to the garnet-rich gneisses (477614, 477608 and 477615) with net mass losses of -25%, -27% and -45 %, respectively.

As mentioned above one garnet-rich gneiss (477607) has immobile element ratios that are intermediate between the amphibolites and the biotite gneiss. This is interpreted as reflecting a sedimentary component in this particular sample. The composition of sample 477607 can be modelled by mixing a basaltic protolith with a sedimentary source, using relative proportions of about 35/65 as estimated by the Zr/TiO_2 ratios (**Fig. 8**). Although it is theoretically possible to use the isocon method to quantify mass changes in such binary rock mixtures, this has not been attempted due to the uncertainty about the actual precursor of sample 477607.

The modelled alteration process results in broadly consistent mass changes for all of the relevant samples, which are intensified as the alteration progresses (**Fig. 9**). There is a general depletion of most major oxides, including SiO_2, $Fe_2O_3^T$, MgO, CaO, Na_2O and P_2O_5. This is compatible with the breakdown of olivine, pyroxenes, plagioclase and apatite in a basaltic precursor. Sr and Ni, which are compatible in plagioclase and olivine, respectively, are also lost. There appears to be a consistent enrichment in K_2O, Cs, Rb, Ba, Pb, Zn, LREE and Th.

6.3. Geological setting and fluid conditions during alteration

A loss of most major elements would be expected if a corrosive fluid reacted with the basaltic precursor rock, and this is also seen in the isocon modelling (**section 6.2**). The observed addition of large ion lithophile elements (LILE) and LREE could represent a second stage of fluid activity, because these elements can be dissolved and mobilised in some aqueous fluids, regardless of the

concentration in the rock with which they are in equilibrium (Mottl and Holland, 1978; Ludden and Thompson, 1979; Staudigel and Hart, 1983; Seyfried et al., 1998). Although, it is not possible to resolve multiple events of alteration with the isocon method, because only the resulting changes can be calculated between two samples, the effects of metamorphism are unlikely to affect the results, because both precursor and altered rocks likely experienced the same metamorphic fluxes.

The mass change calculations suggests that Th was mobile. In this context it should be noted that correct analysis of Th can be difficult, but the fused glass disc method of trace element analysis employed in this study ensures full dissolution of all minerals. Besides, the measured concentrations are well above the detection limit and the Th enrichment is consistently high for all garnet-rich gneiss samples. It is therefore assumed that the calculated Th enrichment is a genuine feature of the alteration process and that it can be used to constrain the conditions of the fluid-rock reaction. Mobility of Th is generally assumed to require the presence of high-temperature supercritical fluids (Kessel et al., 2005). Interestingly, Alt and Teagle (2003) reported addition of Th along with LILE enrichment in the uppermost alteration zone of oceanic seafloor at a fast-spreading ridge in the western Pacific and estimated a temperature below 100°C for the reaction. Below this zone the oceanic crust was also characterised by significant loss of most major elements and the presence of silica-iron deposits. Metasedimentary biotite gneisses on Storø adjacent to the garnet-rich gneiss alteration zone at Storø have Th contents between 4–7.8 ppm (van Gool et al., 2007). These rocks could therefore represent the source of the elevated Th in the garnet-rich gneisses and could also have provided the LILE and LREE enrichment.

The solubility of silica is generally proportional to the temperature of the fluid system (von Damm et al., 1991; Rimstidt, 1997). It is therefore likely that the addition of LILE and LREE took place at low-temperature conditions, since SiO_2 was not added together with these components.

The loss of Fe suggests that the fluid conditions may have been reducing during the alteration, enabling transport of iron as Fe^{2+}. This is consistent with the widely accepted assumption that the Archaean atmosphere and oceans were reduced (Holland, 1984). Furthermore, the presence of an anastomosing network of Fe-rich garnetite within the metasedimentary sequence adjacent to the garnet-rich gneiss (see 'quartz-garnet-magnetite unit', van Gool et al., 2007), could possibly represent redox-induced re-precipitation of Fe that was mobilised during the alteration of the basaltic precursor. Szilas (2008) showed from mass balance considerations that the amount of Fe that was lost in the garnet-rich gneiss alteration zone could indeed account for the observed volume of magnetite precipitated within the metasedimentary sequence as a garnet-magnetite rock. The above mentioned garnet-magnetite rocks possess a seawater-like REE pattern (Szilas, 2008), compatible with the idea that LREE, LILE and Th were added during interaction between seawater and the protolith for the garnet-rich gneiss, after the basaltic precursor had been leached of its major elements during an earlier stage of alteration.

Hydrothermal seafloor alteration (spilitisation) of Archaean basalts has been described by Kitajima et al. (2001) and by Polat et al., (2003, 2007). Generally, the upper alteration zones are strongly carbonated in this type of seafloor alteration, whereas the lower zone is characterised by epidotisation. This bears some resemblance to recent seafloor hydrothermal systems, which are commonly characterised by variable enrichment and depletion of e.g. MgO (chlorite) or Na_2O (albite), depending on what part of the fluid plumbing system is sampled, and on the age of the oceanic crust (Hart, 1970; Hart et al., 1974; Humphris and Thompson, 1978; Seyfried and Bischoff, 1979; Harper, 1999; Paul et al., 2006). This also resembles observations from volcanogenic massive sulfide (VMS) systems, where fluid-rock reaction is controlled by faults and circulation of heated seawater (Franklyn et al., 1981; Lydon, 1984). However, the isocon modelling of the rocks from

453 Storø reported here does not show evidence of either of these two types of alteration, but rather
454 dissolution of the major rock forming minerals.

455 Hofmann (2011) summarised evidence for low-temperature (<150°C) seafloor alteration in the
456 Archaean Barberton greenstone belt in the Kaapvaal craton and demonstrated loss of most major
457 elements and enrichment of LILE and La. However, in this case the altered rocks were also affected
458 by significant silicification. However, no significant addition of SiO_2 is observed for the garnet-rich
459 gneisses at Storø, except in the form of local quartz veins, which may be contemporary with
460 subsequent deformation and metamorphism. A possible explanation of the lack of SiO_2 enrichment
461 is that any dissolved SiO_2 was re-precipitated in the metasedimentary rocks immediately above the
462 alteration zone, whereas Th and LILE were mobilised from the latter rocks to the leached basalts.
463 Alternatively, as discussed above, the fluid temperature might have been low at Storø, SiO_2 being
464 mostly immobile in such conditions.

465 The main remaining question is whether the very significant early leaching of the basaltic
466 precursor (with up to 45% net mass loss) was caused by a low- or high-temperature fluid. Given the
467 occurrence of Au in these supracrustal rocks, it could be suggested that hot epithermal fluids in
468 volcanic systems might have produced the observed net mass changes byadvanced argillic alteration
469 (Hedenquist and Lowenstein, 1994). However, such alteration is commonly also associated with
470 silicification in a vuggy silica cap, which is not observed. Epithermal leaching would also likely
471 have been discordant and would have affected the sedimentary rocks as well. More importantly, the
472 exact age of the volcanic rocks at Storø (bracketed between 2840-2710 Ma) in relation to the
473 earliest Re-Os arsenopyrite age of 2710 Ma (Scherstén et al. 2012) remains unknown, and it is
474 likewise unknown if the initial Au mineralisation might have been epithermal. Primary, discordant
475 hydrothermal plumbing systems might be expected to become transposed into parallellism with the
476 host rocks during ductile deformation and metamorphism, but such systems have nevertheless been

477 recognised in rocks affected by regional deformation and high-grade metamorphism just as intense
478 as in central Storø. A reworked epithermal, Au mineralised alteration system of this type has
479 recently been described from the Qussuk area in northern Godthåbsfjord, only 25–50 km from
480 central Storø (Garde et al., 2012).

481 Deep sea drilling of oceanic crust has documented low-temperature hydrous alteration of oceanic
482 basalts in a process termed seafloor weathering (Robinson et al., 1977; Humphris et al., 1980; Alt,
483 2003). A stepwise increase in the intensity of alteration is observed, with secondary, low-
484 temperature phyllosilicates in the upper crust and hydrous greenschist facies minerals deeper down
485 in the volcanic pile. The alteration process presumably takes place along a chemical gradient that
486 develops during reaction with seawater over millions of years (Wilson et al., 2006). The actual
487 seafloor weathering at any given time is most intense near the free contact to the water column. This
488 is in strong contrast to the fracture- and fluid-flow-controlled types of alteration described above,
489 such as epithermal alteration or spilitisation, which require a convection cell to develop. The
490 qualitative chemical changes deducted from garnet-rich gneiss at central Storø resemble those seen
491 in modern dredged samples from the ocean floor, which consistently show enrichment in LILE and
492 Th, but variable changes in LREE (e.g. Alt and Teagle, 2003). In particular, mass balance
493 calculations of dredged, low-temperature seafloor weathered basalt described by Bienvenu et al.
494 (1990) show a net mass loss of -36% and removal of most major elements in combination with
495 enrichments in LILE and Th (**Fig. 10**).

496 There is also a striking resemblance between the mass changes calculated for the Storø alteration
497 zone (**section 6.2**) and alteration in both recent ocean floor and Permian garnet-chloritoid rocks in
498 Taiwan, which were likewise interpreted to be metamorphosed, seafloor weathered basalts (Yui et
499 al., 1994). **Fig. 10** shows the remarkable similarities between the isocon mass balances for these
500 two alteration zones and those calculated for Storø (**Fig. 9**). The Permian example displays a net

mass loss of -38%, which is in the same range as that calculated for the garnet-rich gneisses on Storø. In both systems most elements were lost, and the enrichments consist of LILE and Th, whereas LREE were either lost or enriched. These complex features may serve to evaluate the specific type of alteration that affected the garnet-rich gneisses at Storø.

We would like to emphasize that the isocon method that we have employed to study these altered rocks can only be applied to the net mass changes when comparing two specific samples. Although it is a possibility that the main mass loss was associated with an earlier stage than the addition of alkali elements, this addition of alkalis is also observed in the two analogue studies to which we compare our data. It therefore seems likely that this type of alteration represents a single commonly occurring process. We simply note that it remains a possibility that the resulting alteration was represented by two events, because we cannot distinguish between the two situations with the applied method. However, we would argue that the entire alteration was caused during low-temperature seawater-rock reaction and we do not invoke a hot hydrothermal system at any stage of the alteration of the mafic rocks to produce these highly aluminous garnet-rich gneisses.

We propose that the main primary alteration product on the island of Storø was montmorillonite, as suggested from the alteration vectors seen in **Fig. 11 and 12**. Montmorillonite is also the predominant alteration mineral in recently drilled samples of modern oceanic crust (e.g. Talbi and Honnorez, 2003; Banerjee et al., 2004). The stability of sericite could account for the enrichment in K_2O, Cs, Rb and Ba, whereas early allanite is a likely accessory phase that could explain the stability of Th and LREE in the altered assemblage. These minerals are typical alteration products and their former presence compatible with the mass changes observed by us from the isocon modelling.

Based on the above characteristics for the alteration system on Storø, we suggest that long-term (several million years) interaction between cold seawater and Meso- to Neoarchaean oceanic crust

525 of island arc affinity resulted in the formation of a clay-rich alteration assemblage during seafloor
526 weathering of the type discussed above. Clastic sediment may have been deposited during the
527 alteration, as indicated by the suggested mixing of altered basalt with sediment displaying distinctly
528 different immobile element ratios (sample 477607). Given the abundance of quartzite in the
529 supracrustal sequence proximity to a continental source seems likely.

530 After accretion of this lithological sequence and adjacent island arc complexes, these rocks
531 where brought to amphibolite facies metamorphic conditions, where the current biotite-garnet-
532 sillimanite assemblage formed. Although such rocks are commonly interpreted in the field as
533 metasedimentary, the present study shows that this may not always be the case. Careful field and
534 geochemical studies may reveal similar seafloor weathered rocks and aluminous rocks affected by
535 other types of premetamorphic alteration in Achaean supracrustal belts world-wide.

536

537 6.4. Implications of the U-Pb zircon geochronology

538

539 The new zircon age data reported here provide evidence that the mafic rocks at central Storø are
540 in fact part of (at least) two distinct sequences. The younger sequence is 2840–2710 Ma in age, as
541 indicated by the youngest detrital U-Pb zircon ages in the metasedimentary biotite gneiss () and the
542 Re-Os age of highly radiogenic arsenopyrite associated with the Au occurrence (van Gool et al.,
543 2007; Scherstén et al., 2012). We propose the formal name the 'Storø Supracrustal Belt' for this
544 younger sequence (<2840 Ma). The older sequence is c. 3050 Ma in age and thus likely genetically
545 related to anorthosite and layered gabbros at Aappalaartoq, from which a similar age is inferred,
546 based on an intrusive tonalitic rock yielding an age of 3053 ± 3.4 Ma (sample 481271, see Hollis et
547 al. 2005). We propose that this older sequence should be termed the 'Storø Anorthosite Complex',

548 so that the allochthonous nature and the different age groups of the mafic and sedimentary rocks on
549 Storø are distinguished in future studies.
550 Together with structural observations reported by van Gool et al. (2007) there is therefore evidence
551 for tectonic juxtaposition of at least two mafic sequences with different ages and tectono-
552 metamorphic histories, as also suggested by Scherstén et al. (2012). A similar tectonic accretion of
553 arc-related supracrustal sequences has also been proposed for the Eoarchaean Isua supracrustal belt
554 north of Godthåbsfjord, supporting an uniformitarian model of continental crust formation for the
555 Godthåbsfjord region (e.g. Nutman and Friend, 2009).
556
557 **7. Summary of key observations and conclusions**
558
559 • Field observations show that garnet-rich gneisses on central Storø contain relict pods and
560 elongate lenses of mafic amphibolite similar to that found in the immediate hanging wall.
561 • Immobile elements (TiO_2, Zr, Hf, Nb, Lu) have similar ratios in the amphibolites and the
562 garnet-rich gneisses, but were residually enriched in the latter rocks due to a net mass loss
563 during alteration.
564 • Isocon mass balance calculations between mafic amphibolite and garnet-rich gneisses
565 suggest that SiO_2, $Fe_2O_3^T$, MgO, CaO, Na_2O, P_2O_5, Sr and Ni were lost during the alteration,
566 consistent with breakdown of rock-forming olivine, pyroxenes, plagioclase and apatite in a
567 basaltic precursor. There appears to be a rather uniform enrichment in K_2O, Cs, Rb, Ba, Pb,
568 Zn, LREE and Th. The net mass loss ranges from -18% to -45%.
569 • Similarities between the calculated mass changes for modern seafloor weathered oceanic
570 basalts and the Archaean rocks studied in this profile at Storø suggest that they represent a

section of fossil ocean floor that was subjected to weathering by long term reaction with cold seawater.

- Seafloor weathering is most intense near the contact with the water column and gradually diminished in intensity with depth. This suggests that the hanging wall amphibolite (unit 1) at central Storø is located stratigraphically below the metasedimentary rocks (unit 3), implying that the sequence might be inverted.
- New U-Pb zircon geochronology confirms that the mafic rocks at Storø comprise at least two rock sequences with distinctly different ages: 1) 'The Storø Supracrustal Belt' (<2840 Ma) and 2) 'The Storø Anorthosite Complex' (c. 3050 Ma).

Acknowledgements

We thank the Bureau of Minerals and Petroleum (BMP), Nuuk, Greenland, for financial support of the field and analytical work and the Geological Survey of Denmark and Greenland (GEUS) for permission to publish this work. We also thank the staff at the Nordsim isotope laboratory, Naturhistoriska Riksmuseet, Stockholm, Sweden, for assistance with zircon geochronology and Dirk Frei and Jørgen Kystol for the geochronology and analytical work performed at GEUS. Comments by Agnete Steenfelt and Feiko Kalsbeek improved the initial manuscript. We thank Patrick Mercier-Langevin and an anonymous reviewer for constructive comments, which also helped to improve this paper. Klaus Mezger is acknowledged for editorial handling. This study is a contribution to IGCP project 599 and Nordsim publication no. **XX**.

References

Alt, J.C., 2003. Hydrothermal fluxes at mid-ocean ridges and on ridge flanks. C.R. Geoscience 335, 853-864.

595 Alt, J.C., Teagle, D.A.H., 2003. Hydrothermal alteration of upper oceanic crust formed at a fast-spreading ridge:
596 mineral, chemical, and isotopic evidence from ODP Site 801. Chemical Geology 201, 191-211.
597 Appel, P.W.U., Garde, A.A., Jørgensen, M.S., Moberg, E., Rasmussen, T.M., Schjøth, F., Steenfelt, A., 2003.
598 Preliminary evaluation of the economic potential of greenstone belts in the Nuuk region. Danmarks og Grønlands
599 Geologiske Undersøgelse Rapport 2003/94, 147 pp.
600 Banerjee, N.R., Honnorez, J., Muehlenbachs, K., 2004. Low-temperature alteration of submarine basalts from the
601 Ontong Java Plateau. In. Fitton, J.G., Wallace, J.J., Saunders, P.J. (eds.), Origin and evolution of the Ontong Java
602 Plateau. Geological Society of London, Special Publications 229, 259-273.
603 Beech, E.M., Chadwick, B., 1980. The Malene supracrustal gneisses of northwest Buksefjorden: their origin and
604 significance in the Archaean crustal evolution of southern West Greenland. Precambrian Research 11, 329-355.
605 Bienvenu, P., Bougault, H., Joron, J.L., Treuil, M., Dmitriev, L., 1990. MORB alteration: rare-earth element/non-rare-
606 earth hygromagmaphile element fractionation. Chemical Geology 82, 1-14.
607 Bolhar, R., Kamber, B.S., Moorbath, S., Whitehouse, M.J., Collerson, K.D., 2005. Chemical characterization of earth's
608 most ancient clastic sediments from the Isua Greenstone Belt, southern West Greenland. Geochimica et
609 Cosmochimica Acta 69, 1555-1573.
610 Bonnet, A.-L., Corriveau, L., La Fléche, M.R., 2005. Chemical imprint of highly metamorphosed volcanic-hosted
611 hydrothermal alterations in the La Romaine Supracrustal Belt, eastern Grenville Province, Quebec. Canadian
612 Journal of Earth Science 42, 1783-1814.
613 Brown, M., Friend, C.R.L., McGregor, V.R., Perkins, W.T. 1981. The late Archaean Qörqut granite complex of
614 southern West Greenland. Journal of Geophysical Research 86, 10617–10632.
615 Dymek, R.F., Smith, M.S., 1990. Geochemistry and origin of Archaean quartz-cordierite gneisses from the
616 Godthåbsfjord region, West Greenland. Contributions to Mineralogy and Petrology 105, 715-730.
617 Eilu, P., Groves, D.I., 2001. Primary alteration and geochemical dispersion haloes of Archaean orogenic gold deposits
618 in the Yilgarn Craton: the pre-weathering scenario. Geochemistry: Exploration, Environment, Analysis 1, 183-200.
619 Eilu, P., Garofalo, P., Appel, P.W.U., Heijlen, W., 2006. Alteration patterns in Au-mineralised zones of Storø, Nuuk
620 region - West Greenland. Danmarks og Grønlands Geologiske Undersøgelse Rapport 2006/30, 73 pp.
621 Franklin, J.M., Lydon, J.W. Sangster, D.F.. 1981. Volcanic-associated massive sulfide deposits." Economic Geology
622 75, 485-627.

623 Frei, D., Gerdes, A. 2009. Precise and accurate in situ U-Pb dating ofzircon with high sample throughput by automated
624 LA-SF-ICP-MS. Chemical Geology 261, 261-270.
625 Friend, C.R.L., Nutman, A.P., McGregor, Kinny, P.D., McGregor, V.R., 1996. Timing of late Archaean terrane
626 assembly, crustal thickening and granite emplacement in the Nuuk region, southern West Greenland. Earth
627 Planetary Science Letters 142, 353–365.
628 Garde, A.A., 1987. Geological Map of Greenland, 1:100 000, Isukasia 65 V.2 Syd. Geological Survey of Greenland,
629 Copenhagen.
630 Garde, A.A., 1989. Geological Map of Greenland, 1:100 000, Fiskefjord 64 V.1 Nord. Geological Survey of Greenland,
631 Copenhagen.
632 Garde, A.A., 2007. A mid-Archaean island arc complex in the eastern Akia terrane, Godthåbsfjord, southern West
633 Greenland. Journal of the Geological Society, London, 164, 565-579.
634 Garde, A.A., Stendal, H., Stensgaard, B.M., 2007. Pre-metamorphic hydrothermal alteration with gold in a mid-
635 Archaean island arc, Godthåbsfjord, West Greenland. Geological Survey of Denmark and Greenland Bulletin 13,
636 37-40.
637 Garde, A.A., Whitehouse, M., Christensen, R., 2012. Mesoarchean epithermal gold mineralization preserved at upper
638 amphibolite-facies grade, southern West Greenland. Economic Geology 107, 1-29.
639 Goldfarb, R.J., Groves, D.I., Gardoll, S., 2001. Orogenic gold and geologic time: a global synthesis. Ore geology
640 reviews 18, 1-75.
641 Grahl-Madsen, L., 1994. Storø gold project, Southwest Greenland 1994. Internal report by NunaOil A/S. Geological
642 Survey of Denmark and Greenland Report file 21413, 20 pp.
643 Gresens, R.L., 1967. Composition-volume relationships of metasomatism. Chemical Geology 2, 47-55.
644 Grant, J.A., 1986. The isocon diagram – a simple solution to Gresens' equation for metasomatic alteration. Economic
645 Geology 81, 1976-1982.
646 Grant, J.A., 2005. Isocon analysis: a brief review of the method and applications. Physics and Chemistry of the Earth
647 30, 997-1004.
648
649 Groves, D.I., Goldfarb, R.J., Robert., F., Hart, C.J.R., 2003. Gold Deposits in Metamorphic Belts: Overview of Current
650 Understanding, Outstanding Problems, Future Research, and Exploration Significance. Economic Geology 98, 1-29.

651 Hallberg, A., 1993. The Enåsen gold deposit, central Sweden. 1. A palaeoproterozoic high-sulphidation epithermal gold
652 mineralization. Mineralium Deposita 29, 150-162.
653 Hart, R., 1970. Chemical exchange between sea water and deep ocean basalts. Earth and Planetary Science Letters 9,
654 269-279.
655 Hart, S.R., Erlank, A.J., Kable, E.J.D., 1974. Sea floor basalt alteration: some chemical and Sr isotopic effects.
656 Contributions to Mineralogy and Petrology 44, 219-230.
657 Harper, G.D., 1999. Structural styles of hydrothermal discharge in ophiolite/sea floor systems. Reviews in Economic
658 Geology 8, 53-73.
659 Hedenquist, J.W., Lowenstein, J.B., 1994. The role of magmas in the formation of hydrothermal ore deposits. Nature
660 370, 519–527
661 Herrmann, W., Berry, R.F., 2002. MINSQ – a least squares spreadsheet method for calculating mineral proportions
662 from whole rock major element analysis. Geochemistry: Exploration, Environment, Analysis 2, 361-368.
663 Herron, M.M., 1988. Geochemical classification of terrigeneous sands and shales from core or log data. Journal of
664 Sedimentary Petrology 58, 820-829.
665 Hofmann, A., 2011. Archaean hydrothermal systems in the Barberton Greenstone Belt and their significance as a
666 habitat for early life. In: Golding, S.D., Glikson, M. (eds.), Earliest life on Earth: habitats, environments and
667 methods of detection. Springer Science and Business Media, 51-78.
668 Holland, H.D., 1984. The chemical evolution of atmosphere and oceans. Princeton University Press, 351 pp.
669 Hollis, J.A. (ed.), 2005. Greenstone belts in the central Godthåbsfjord region, southern West Greenland: geochemistry,
670 geochronology and petrography arising from 2004 field work, and digital map data. Danmarks og Grønlands
671 Geologiske Undersøgelse Rapport 2006/45, 56 pp.
672 Humphris, S.E., Thompson, G., 1978. Hydrothermal alteration of oceanic basalts by seawater. Geochimica et
673 Cosmochimica Acta 42, 107-125.
674 Humphris, S.E., Melson, W.G., Thompson, R.N., 1980. Basalt weathering on the East Pacific Rise and Galapagos
675 spreading center, Deep Sea Drilling Project leg 54. In: Rosendahl, B.R., Hekinian, R., et al., Init. Repts. DSDP 54,
676 773-787.
677 Irvine, T.N. and Baragar, W.R.A., 1971. A guide to the chemical classification of the common volcanic rocks. Canadian
678 Journal of Earth Science 8, 523-548.

679 Janoušek, V., Farrow, C.M., Erban, V., 2006. Interpretation of whole-rock geochemical data in igneous geochemistry:
680 introducing Geochemical Data Tool (GCDkit). Journal of Petrology 47, 1255-1259.
681 Jensen, L.S., 1976. A new cation plot for classifying subalkalic volcanic rocks. Ontario Division of Mines,
682 Miscellaneous Paper 66, 22 pp.
683 Juul-Pedersen, A., Frei, R., Appel, P.W.U., Persson, M.F., Konnerup-Madsen, J., 2007. A shear zone related greenstone
684 belt hosted gold mineralization in the Archean of West Greenland. A petrographic and combined Pb-Pb and Rb-Sr
685 geochronological study. Ore Geology Reviews 32, 20-36.
686 Kessel, R., Schmidt, M.W., Ulmer, P., Pettke, T., 2005. Trace element signature of subduction-zone fluids, melts and
687 supercritical liquids at 120-180 km depth. Nature 437, 724-727.
688 Kitajima, K., Maruyama, S., Utsunomiya, S., Liou, J.G., 2001. Seafloor hydrothermal alteration at an Archaean mid-
689 ocean ridge. Journal of Metamorphic Geology 19, 583-599.
690 Knudsen, C., van Gool, J.A.M., Østergaard, C., Hollis, J.A., Rink-Jørgensen, M., Persson, M., Szilas, K., 2007. Gold-
691 hosting supracrustal rocks on Storø, southern West Greenland: lithologies and geological environment. Geological
692 Survey of Denmark and Greenland Bulletin 13 , 41-44.
693 Kystol, J. Larsen, L.M., 1999. Analytical procedures in the Rock Geochemical Laboratory of the Geological Survey of
694 Denmark and Greenland. Geology of Greenland Survey Bulletin 184, 59-62.
695 López-Moro, F.J., 2012. EASYGRESGRANT – A Microsoft Excel spreadsheet to quantity volume changes and to
696 perform mass-balance modelling in metasomatic systems. Computer and Geosciences 39, 191-196.
697 Ludden, J.N., Thompson, G., 1979. An evaluation of the behaviour of the rare earth elements during the weathering of
698 sea-floor basalts. Earth and Planetary Science Letters 43, 85-92.
699 Ludwig, K.R., 2003. Isoplot/Ex 3.00. A Geochronological Toolkit for Microsoft Excel. Special Publication 4. Berkeley
700 Geochronological Center, Berkeley, CA.
701 Lydon, J.W., 1984, Volcanogenic massive sulphide deposits Part 1: A descriptive model: Geoscience Canada 11, 195-
702 202.
703 McFarlane, C.R.M., Mavrogenes, J.A., Tomkins, A.G., 2007. Recognizing hydrothermal alteration through a granulite
704 facies metamorphic overprint at the Challenger Au deposit, South Autralia. Chemical Geology 243, 64-89.
705 Miyashiro, A., 1974. Volcanic rock series in island arcs and active continental margins. American Journal of Science
706 274, 321-355.

Mottl, M.J., Holland, H.D., 1978. Chemical exchange during hydrothermal alteration of basalt by seawater-I. Experimental results for major and minor components of seawater. Geochimica et Cosmochimica Acta 42, 1103-1115.

Nutman, A.P., McGregor, V.R., Friend, C.R.L., Bennett, V.C., Kinny, P.D., 1996. The Itsaq Gneiss Complex of southern West Greenland; the world's most extensive record of early crustal evolution (3900-3600 Ma). Precambrian Research 78, 1-39.

Nutman, A.P., Friend, C.R.L., 2007. Adjacent terranes with ca. 2715 and 2650 Ma high-pressure metamorphic assemblages in the Nuuk region of the North Atlantic Craton, southern West Greenland: complexities of Neoarchaean collisional orogeny. Precambrian Research 155.

Nutman, A.P., Christiansen, O., Friend, C.R.L., 2007. 2635 Ma amphibolite facies gold mineralisation near a terrane boundary (suture?) on Storø, Nuuk region, southern West Greenland. Precambrian Research 159, 19-32.

Nutman, A.P., Friend, C.R.L., 2009. New 1:20,000 scale geological maps, synthesis and history of investigation of the Isua supracrustal belt and adjacent orthogneisses, southern West Greenland: A glimpse of Eoarchaean crust formation and orogeny. Precambrian Research 172, 189-211.

Nutman, A.P., Friend, C.R.L., Hiess, J., 2010. Setting of the ~2560 Ma Qôrqut Granite Complex in the Archaean crustal evolution of southern West Greenland. Amercian Journal of Science 310, 1081-1114.

Ohta, T., Arai, H., 2007. Statistical empirical index of chemical weathering in igneous rocks: A new tool for evaluating the degree of weathering. Chemical Geology 240, 280-297.

Ordóñez-Calderón, J.C., Polat, A., Fryer, B.J., Gagnon, J.E., 2011. Field and geochemical characteristics of Mesoarchean to Neoarchean volcanic rocks in the Storø greenstone belt, SW Greenland: Evidence for accretion of intra-oceanic volcanic arcs. Precambrian Research 184, 24-42.

Østergaard, C., van Gool, J.A.M., 2007. Assessment of the gold mineralisation on Storø, Godthåbsfjord, southern West Greenland. Danmarks og Grønlands Geologiske Undersøgelse Rapport 2007/78, 20 pp.

Owens, B.E., Pasek, M.A, 2007. Kyanite quartzites in the Piedmont Province of Virginia: evidence for a possible high-sulfidation system. Economic Geology 102, 495-509.

Paul, H.J., Gillis, K.M., Coggon, R.M., Teagle, D.A.H., 2006. ODP site 1224: a missing link in the investigation of seafloor weathering. Geochemistry, Geophysics, Geosystems 7, Q023003, 15 pp.

Pedersen, N.H., 1996. Guldmineraliseringer på Storø, Sydlige Vestgrønland. Progress report, forskeruddannelse del A. Geologisk Institut, Århus University. GEUS report file 22029, 83 pp.

736 Penczak, R.S., Mason, R., 1999. Characteristics and origin of Archaean premetamorphic hydrothermal alteration at the
737 Campbell gold mine, Northwestern Ontario, Canada. Economic Geology 94, 507-528.
738 Persson, M.F., 2007. Metamorphic and geochronological evolution of the Au-bearing rocks on central Storø, Nuuk
739 region, West Greenland. Unpublished M.Sc. thesis, University of Copenhagen, 91 pp.
740 Polat, A., Hofmann, A.W., Münker, C., Regelous, M., Appel, P.W.U., 2003. Constrasting geochemical patterns in the
741 3.7-3.8 Ga pillow basalt cores and rims, Isua greenstone belt, Southwest Greenand: Implications for postmagmatic
742 alteration processes. Geochimica et Cosmochimica Acta 67, 441-457.
743 Polat, A., Appel, P.W.U., Frei, R., Pan, Y., Dilek, Y., Ordóñez-Calderón, Fryer, B., Hollis, J.A., Raith, J., 2007. Field
744 and geochemical characteristics of the Mesoarchaean (~3075 Ma) Ivisaartoq greenstone belt, southern West
745 Greenland: evidence for seafloor hydrothermal alteration in supra-subduction zone oceanic crust. Gondwana
746 Research 11, 69–91.
747 Polat, A., Longstaffe, F., Weisener, C., Fryer, B., Frei, R., Kerrich, R., 2012. Extreme element mobility during
748 transformation of Neoarchean (ca. 2.7 Ga) pillow basalts to a Paleoproterozoic (ca. 1.9 Ga) paleosol, Schreiber
749 Beach, Ontario, Canada. Chemical Geology 326-327, 145-173.
750 Rimstidt, J.D., 1997. Gangue mineral transport and deposition. In: Barnes, H.L. (ed.), Geochemistry of hydrothermal
751 ore depositis, third edition. Wiley and Sons, 487-516.
752 Rivalenti, G., Rossi, A., 1972. The geology and petrology of the Precambrian rocks to the north-east of the fjord
753 Qagssit, Frederikshåb district, South-West Greenland. Grønlands Geologiske Undersøgelse Bulletin 103, 95 pp.
754 Robinson, P.T., Flower, M.F.J., Schminke, H.-U., et al., 1977. Low temperature alteration of oceanic basalts, DSDP leg
755 37. In Aumento, F., Melson, W.G., et al., Init. Repts., DSDP 37, 775-794.
756 Scherstén, A., Szilas, K., Creaser, R.A., van Gool, J.A.M., Næraa, T., Østergaard, C., 2012. Re-Os and U-Pb constraints
757 on gold mineralisation events in the Meso- to Neoarchaean Storø greenstone belt, Storø, southern West Greenland.
758 Precambrian Research 200-203, 149-162.
759 Schiøtte, L.. Compston, W., Bridgwater, D., 1989. U–Th–Pb ages of single zircons in Archaean supracrustals from Nain
760 Province, Labrador, Canada. Canadian Journal of Earth Sciences 26, 2636-2644.
761 Schiøtte, L., Bridgwater, D., 1990. Multi stage late Archaean granulite facies metamorphism in northern Labrador,
762 Canada. In: Vielzeuf, D. Vidal, P. (eds.), Granulites and Crustal Evolution, NATO ASI Ser. C: Mathematical and
763 Physical Sciences, Kluwer, Dordrecht, 157-169.

764 Seyfried, W.E.Jr., Bischoff, J.L., 1979. Low temperature basalt alteration by seawater: an experimental study at 70°C
765 and 150°C. Geochimica et Cosmochimica Acta 43, 1937-1947.
766 Seyfried, W.E., Chen, X., Chan, L.-H., 1998. Trace element mobility and lithium isotope exchange during hydrothermal
767 alteration of seafloor weathered basalt: An experimental study at 350°C, 500 bars. Geochimica et Cosmochimica
768 Acta 62, 949-960.
769 Skyseth, T., 1996. Gold exploration on Storø, South West Greenland. Exploration license 13/97. Company report by
770 NunaOil A/S. Geological Survey of Denmark and Greenland Report file 21565, 359 pp.
771 Smith, M.S., Dymek, R.F., Chadwich, B., 1992. Petrogenesis of Archaean Malene supracrustal rocks, NW
772 Buksefjorden region, West Greenland: geochemical evidence for highly evolved Archaean crust. Precambrian
773 Research 57, 49-90.
774 Stacey, J.S., Kramers, J.D., 1975. Approximation of terrestrial lead isotope evolution by a two-stage model. Earth and
775 Planetary Science Letters 26, 207-221.
776 Staudigel, H., Hart, S.R., 1983. Alteration of basaltic glass: Mechanisms and significance for the oceanic crust-seawater
777 budget. Geochimica et Cosmochimica Acta 47, 337-350.
778 St.-Onge, M., van Gool, J. A. M., Garde, A. A., Scott, D. J. 2009. Correlation of Archaean and Palaeoproterozoic units
779 between northeastern Canada and western Greenland: constraining the pre-collisional upper plate accretionary
780 history of the Trans-Hudson orogen. In: Cawood, P. A. & Kroner, A. (eds) Accretionary Orogens in Space and
781 Time. Geological Society, London, Special Publications 318, 193–235.
782 Sun, S., McDonough, W.F., 1989. Chemical and isotopic systematics of oceanic basalts: implications for mantle
783 composition and processes. In: Saunders, A.D., Norry, M.J. (eds.), Magmatism in the Ocean Basins. Geological
784 Society of London, Special Publications 42, 313-345.
785 Szilas, K., 2008. Geochemistry of the late Archaean Storø supracrustal belt and alteration zones associated with gold
786 mineralisation, Nuuk region, southern West Greenland. Unpublished M.Sc. thesis, University of Copenhagen, 42 pp.
787 Szilas, K., Hoffmann, J.E., Scherstén, A., Rosing, M.T., Kokfelt, T.F., Windley, B.F., van Hinsberg, V.J., Næraa, T.,
788 Keulen, N., Frei, R., Münker, C., 2012. Complex calc-alkaline volcanism recorded in Mesoarchaean supracrustal
789 belts north of Frederikshåb Isblink, southern West Greenland: implications for subduction zone processes in the
790 early Earth. Precambrian Research 208-211, 90-123.

Szilas, K., van Hinsberg, J., Kisters, A.F.M., J. Hoffmann, E., Kokfelt, T.F., Scherstén, A., Windley, B.F., Münker, C., 2013a. Remnants of arc-related Mesoarchaean oceanic crust in the Tartoq Group, SW Greenland. Gondwana Research 23, 436-451.

Szilas, K., Hoffmann, J.E., Scherstén, A., Kokfelt, T.F, Münker, C., 2013b. Archaean andesite petrogenesis: insights from the Grædefjord supracrustal belt, SW Greenland. Precambrian Research (in press).Talbi, El Hassan, Honnorez, J., 2003. Low-temperature alteration of Mesozoic oceanic crust, Ocean Drilling Program Leg 185. Geochemistry, Geophysics, Geosystems 4, 8906, 21 pp.

Trepka-Bloch, C., 1996. Gold exploration Storø 1995. Exploration license 02/92. Company report by NunaOil A/S. Geological Survey of Denmark and Greenland Report file 218323, 39 pp.

van Gool, J.A.M., Scherstén, A., Østergaard, C., Neraa, T., 2007. Geological setting of the Storø gold prospect, Godhåbsfjord region, southern West Greenland. Danmarks og Grønlands Geologiske Undersøgelse Rapport 2007/83, 150 pp.

von Damm, K.L., Bischoff, J.L., Rosenbauer, R.J., 1991. Quartz solubility in hydrothermal seawater: an experimental study and equation describing quartz solubility for up to 0.5 M NaCl solutions. American Journal of Science 291, 977-1007.

Whitehouse, M.J., Kamber, B.S. 2005. Assigning dates to thin gneissic veins in high-grade metamorphic terranes - a cautionary tale from Akilia, southwest Greenland: Journal of Petrology 46, 291-318.

Whitehouse M.J., Kamber B., and Moorbath S. 1999. Age significance of U-Th-Pb zircon data from early Archaean rocks of west Greenland – a reassessment based on combined ion-microprobe and imaging studies: Chemical Geology 160, 201-224.

Wilson, D.S., Teagle, D.A.H., Alt, J.C., et al., 2006. Drilling to gabbro in intact oceanic crust. Science 321, 1016-1020.

Windley, B.F., Garde, A.A., 2009. Arc-generated blocks with crustal sections in the North Atlantic craton of West Greenland: Crustal growth in the Archean with modern analogues. Earth-Science Reviews 93, 1-30.

Yui, T.-F., Wu., T.-W., Wang, Y., Lo, C.-H., Lu, C.-Y., 1994. Evidence for submarine weathering from metamorphosed weathering profiles on basaltic rocks, Tanao Metamorphic Complex, Taiwan. Chemical Geology 118, 185-202.

Figure text

Fig. 1. Geological map of the Godthåbsfjord region in southern West Greenland with the location of the study area on the island of Storø. Based in part on Garde (1987, 1989).

Fig. 2. Geological map of central Storø, modified from Fig. 1 in van Gool et al. (2007). The positions of localities 79, 80 and 83 mark the geographical top, middle and bottom of the profile from which field observations and geochemical data are presented.

Fig. 3. Field photographs of metasedimentary, metavolcanic and garnet-rich, chemically altered aluminous rock units at 'Lille Qingaaq' (lower peak of Qingaaq mountain), central Storø. **a**. Fragmental amphibolite of likely volcaniclastic origin. Loc. 79. **b**. Contact between mafic metavolcanic amphibolite and altered, garnet-rich aluminous rock. Loc. 79. The garnet-rich gneiss visible in the right part of Fig. 3b contains up to 40% almandine garnet, 20–30% plagioclase, biotite and commonly sillimanite, and is generally quartz-poor. **c-d**. Pods of relict amphibolite in altered, garnet-rich rocks. Note gradational boundaries, variable garnet content in relict pods, absence of partial melting, and fold in Fig. 3d. Loc. 80. **e-f**. Metagreywacke with quartz veins and partial melt veins. Loc. 80. **g**. Finely layered amphibolite of andesitic composition, interpreted as having a pyroclastic protolith. Loc. 83. **h**. Felsic layer in finely layered amphibolite. Loc. 83. The size of the coin is 24.5 mm in diameter.

Fig. 4. MFW-weathering index of Ohta and Arai (2007), showing that the amphibolites and the layered amphibolite plot along the igneous trend, whereas the biotite gneiss and the garnet-rich gneisses plot in the field of weathered and/or altered rocks.

Fig. 5. Primitive mantle-normalised (Sun and McDonough, 1989) trace element diagrams for the various lithological units presented in this study. a) Amphibolite, b) garnet-rich gneiss, c) biotite

gneiss and d) dacitic component within layered amphibolite. The shaded area is the total range of all samples.

Fig. 6. Profile from the least altered amphibolite, across the garnet-rich gneiss and into the biotite gneiss, showing variations in Zr/TiO_2 and A/CNK (Al/(Ca+Na+K).

Fig. 7. **a**. CL (cathodoluminescence) and BSE (backscattered electron) images showing typical morphology of igneous zircon in sample 477618 (felsic layer in layered amphibolite) and detrital and metamorphic zircon in sample 477609 (metasedimentary biotite gneiss). Note igneous-type oscillatory zoning and sector zoning in 477618, and zoned crystal fragments with homogeneous metamorphic overgrowths as well as entire homogeneous grains in 477609. **b-c**. U-Pb concordia diagrams for samples 477618 and 477609 showing age distributions. Scale bar is 100 microns in all images.

Fig. 8. Plots of various high field strength elements showing the similar trend for the amphibolites and the garnet-rich gneisses. Biotite gneiss shown for comparison, shows a distinctly different trend. TiO_2 is in wt.% and Zr, Hf, Nb and Lu are in ppm.

Fig. 9. Isocon mass balance calculations for the alteration of the garnet-rich gneisses from a median basaltic precursor. It is assumed that TiO_2, Zr, Hf, Nb and Lu remained immobile during the alteration. The calculations were performed in the EASYGRESGRANT Microsoft Excel spread sheet program of López-Moro (2012). The results are plotted here as loss/gain relative to the precursor ($\Delta C_i/C_i^o$). The absolute loss/gain (ΔC_i) in wt.% or ppm are reported in the supplementary Table 3.

867

868 Fig. 10. Isocon mass balance calculations for a sample pair from Yui et al. (1994) and Bienvenu et
869 al. (1990). The results are plotted here as loss/gain relative to the precursor ($\Delta C_i/C_i^o$).

870

871 Fig. 11. Amphibolites (squares), Garnet-rich gneisses (triangles) and montmorillonite and sericite
872 end-members (crosses) showing possible trends from of the garnet-rich gneisses from the
873 amphibolites towards these common alteration products. End-members are taken from Herrmann
874 and Berry (2002) and normalised to 100% on a volatile-free basis.

875

876 Fig. 12. Ternary diagram of the amphibolite, garnet-rich gneisses and possible alteration end-
877 members. The distinct trends towards the clay end-members suggests equilibrium change towards
878 these components during the alteration process.

879

880 **Supplementary Data Tables**

881 Table 1. Major and trace element geochemical data for the samples.

882

883 Table 2. U-Pb isotope data for zircon.

884

885 Table 3. Isocon mass balance calculations.

Figure 1

Click here to download high resolution image

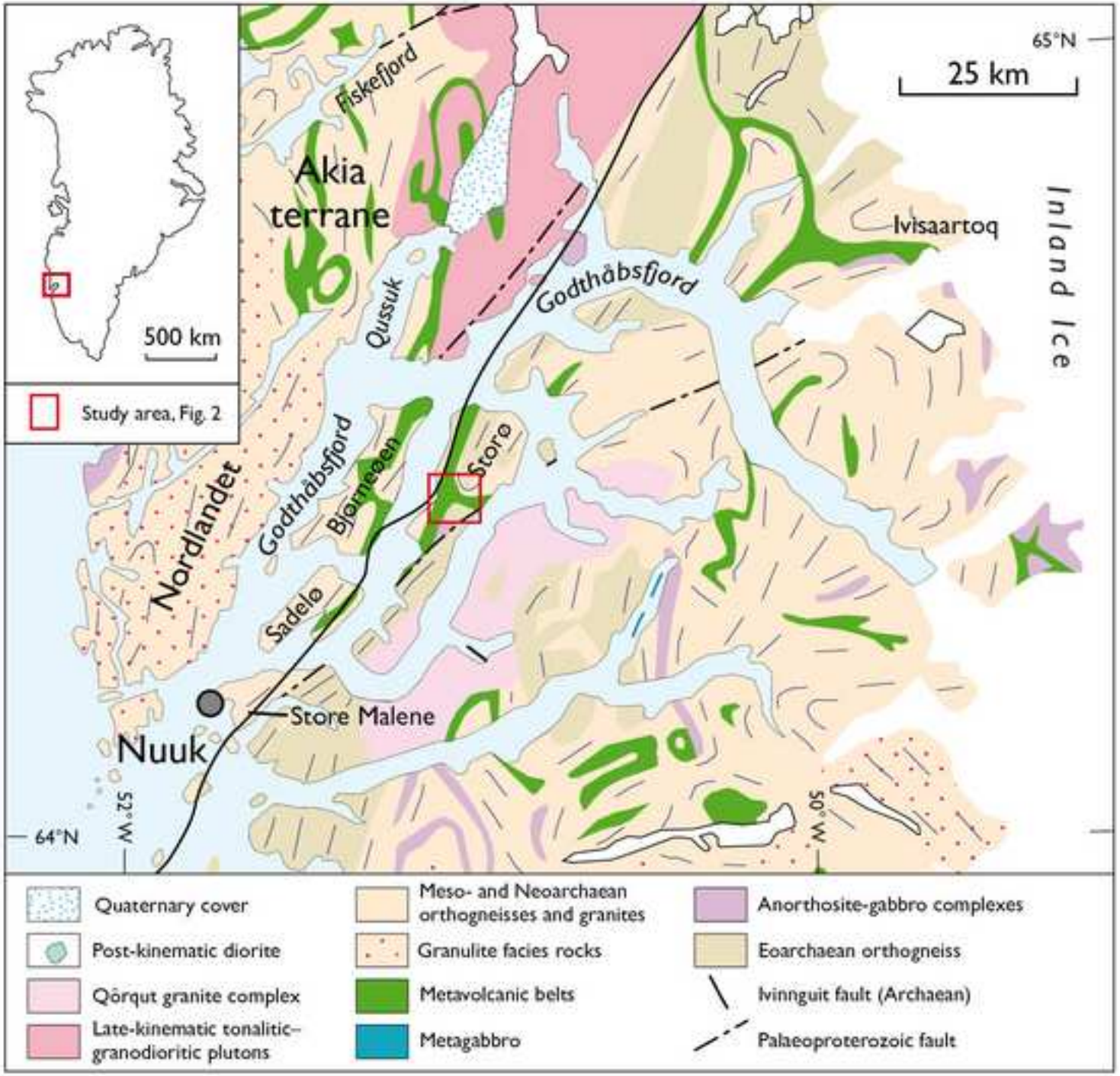

Figure 2

Click here to download high resolution image

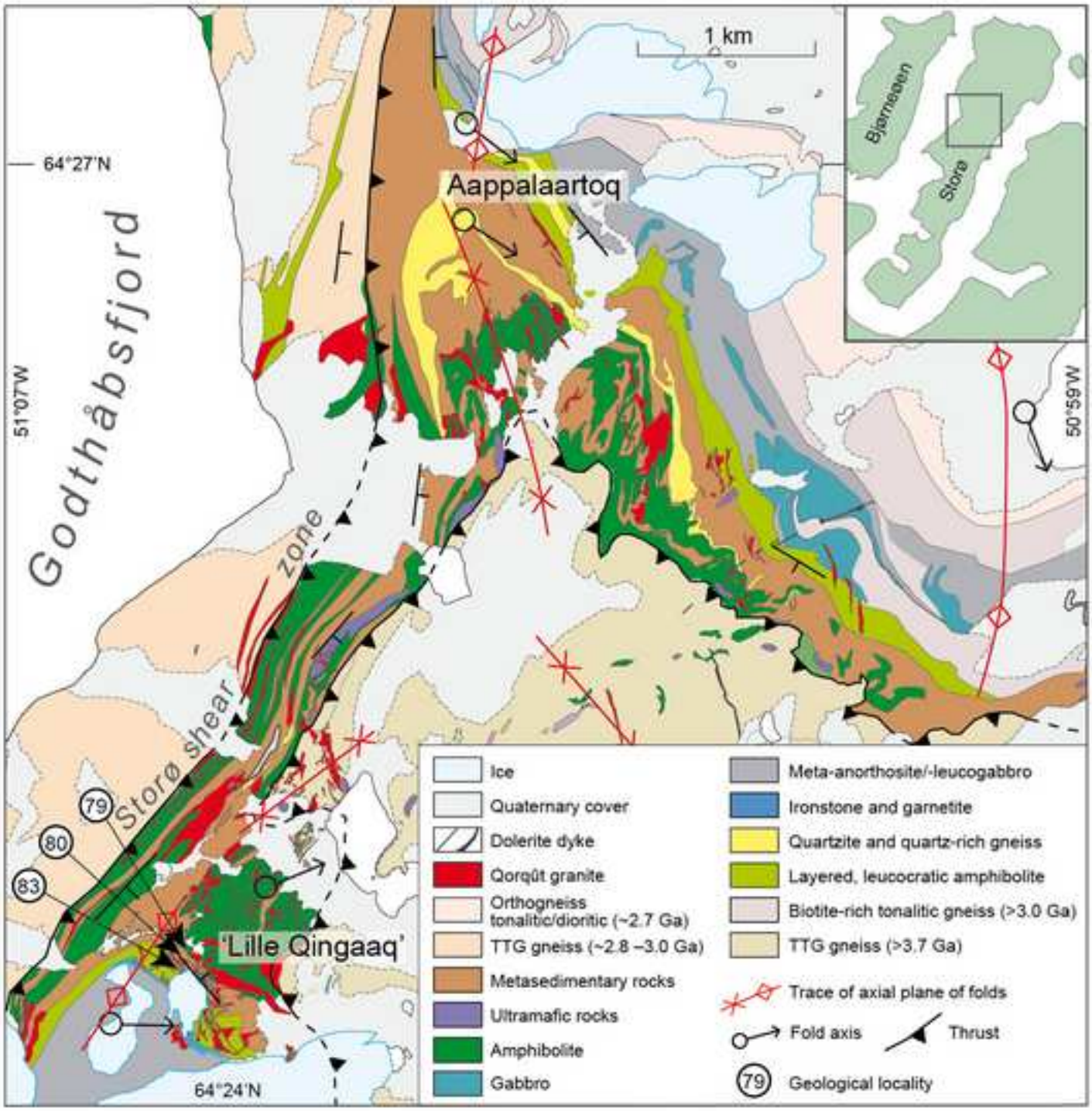

Figure 3

Click here to download high resolution image

Figure 4

Click here to download high resolution image

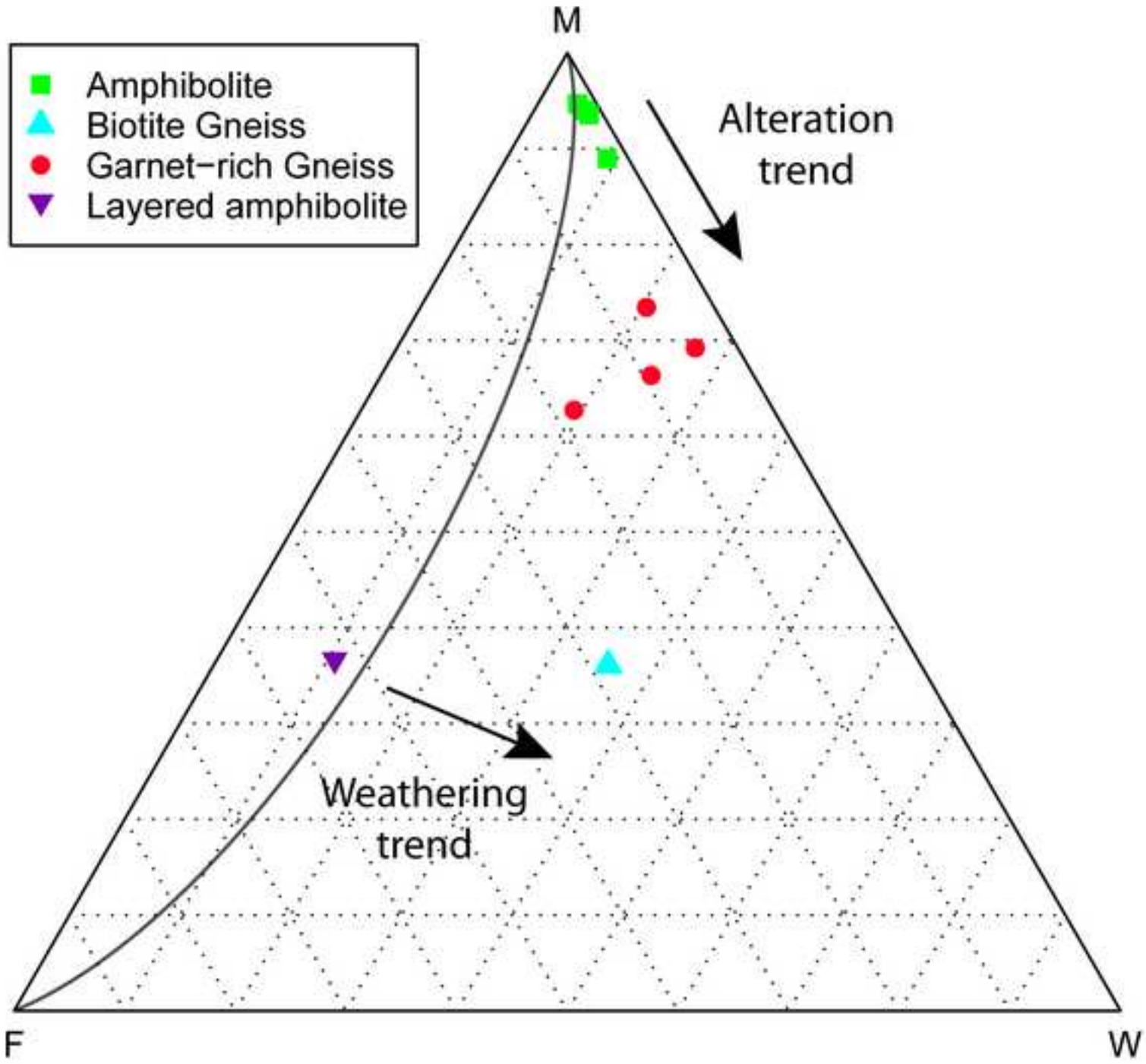

Figure 5

Click here to download high resolution image

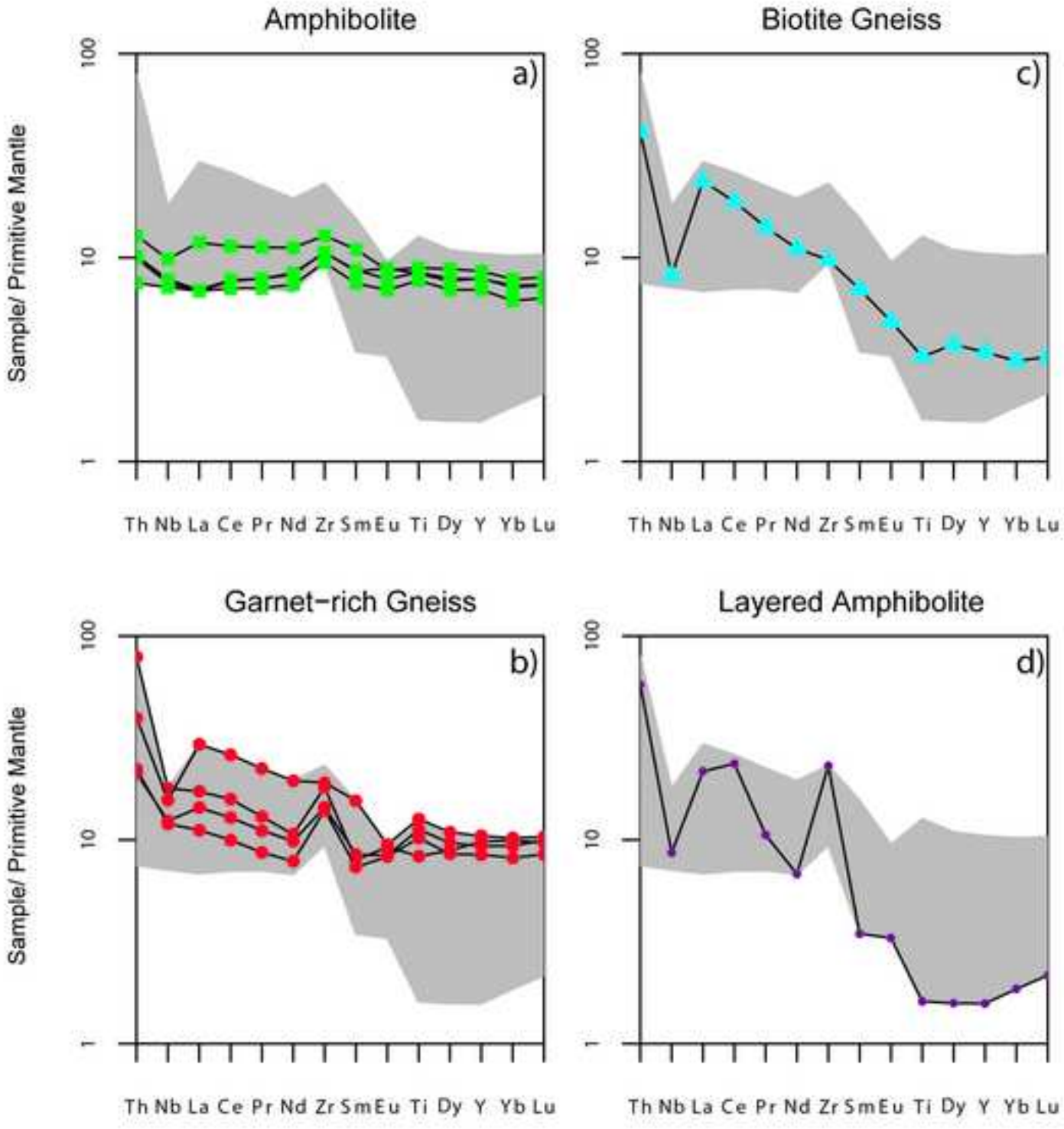

Figure 6

Click here to download high resolution image

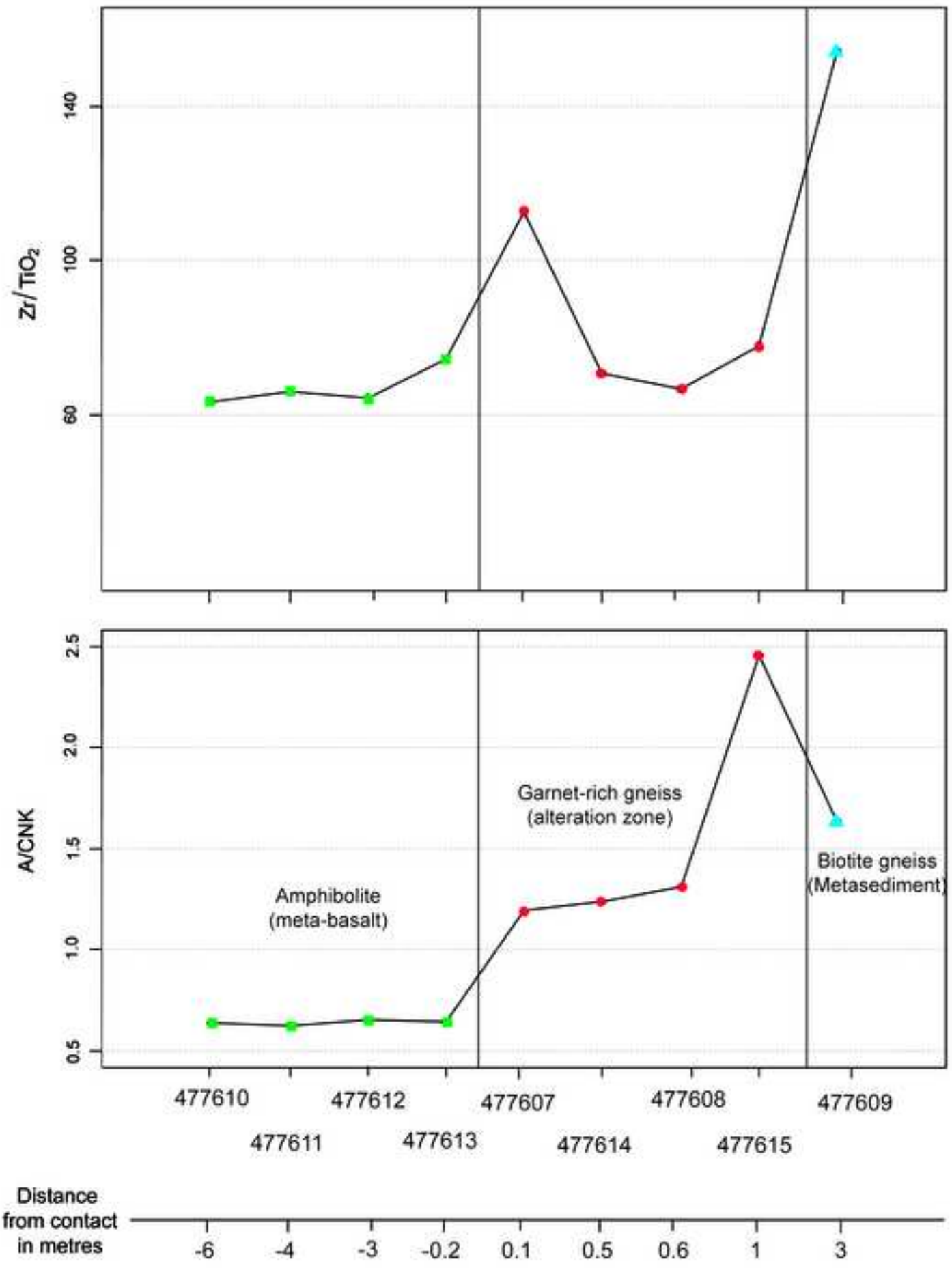

Figure 7a

Click here to download high resolution image

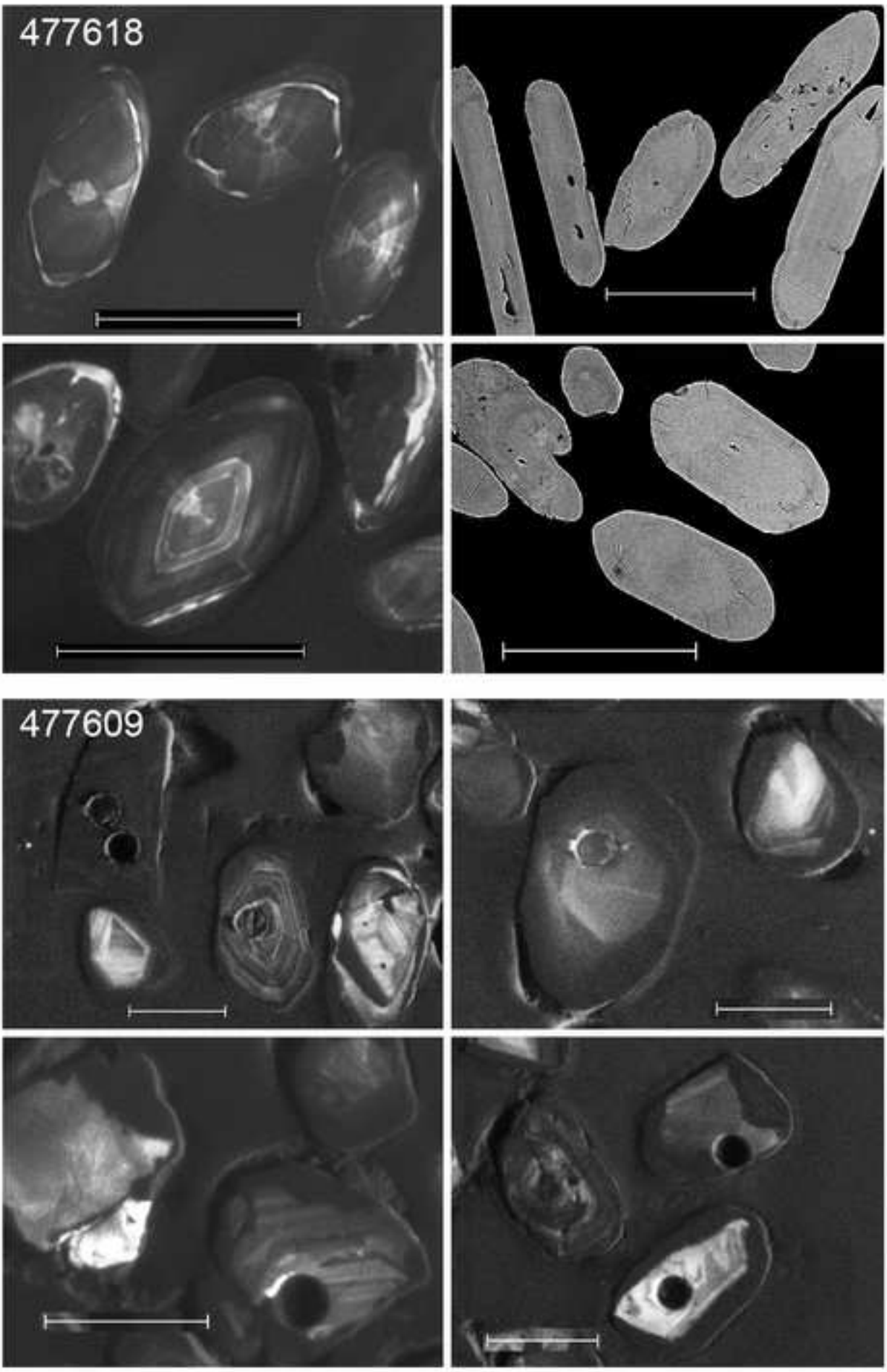

Figure 7bc

Click here to download high resolution image

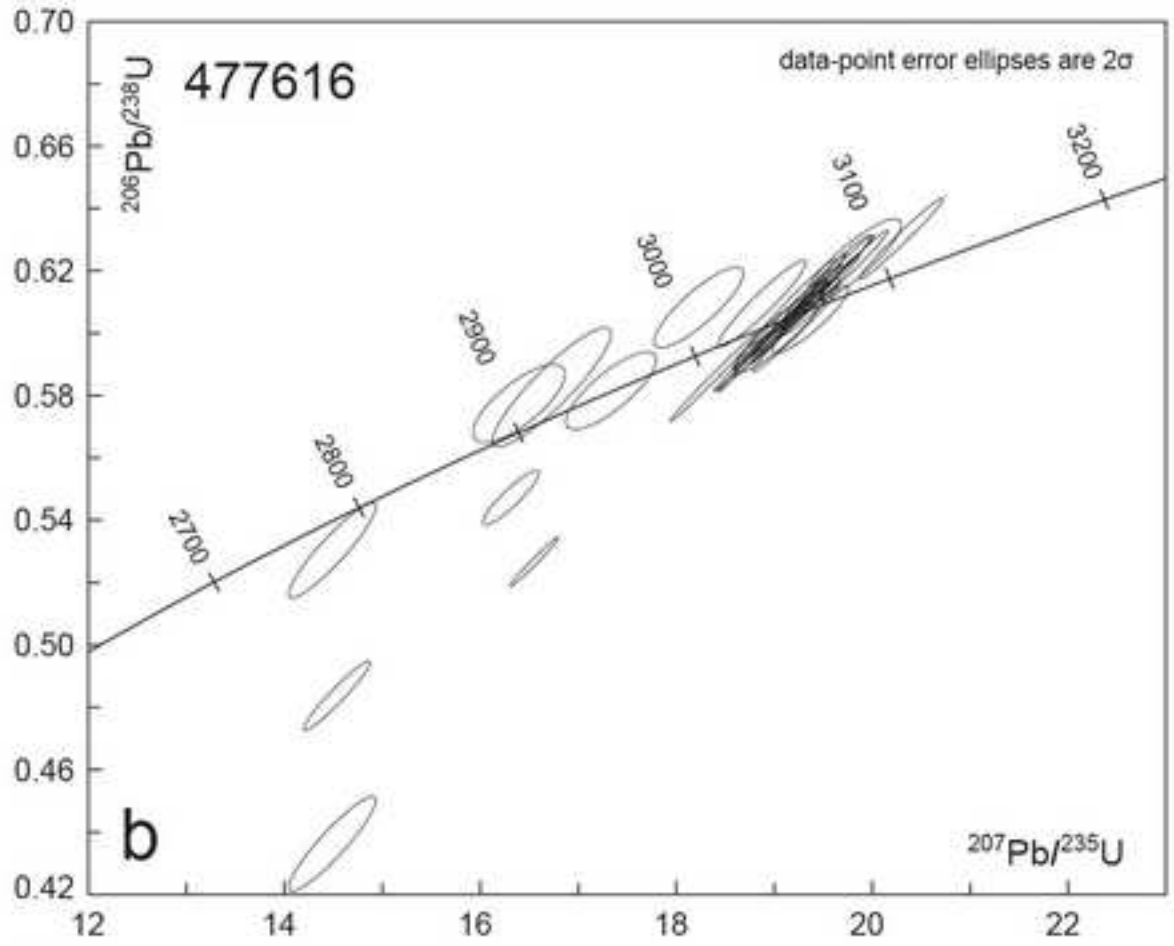

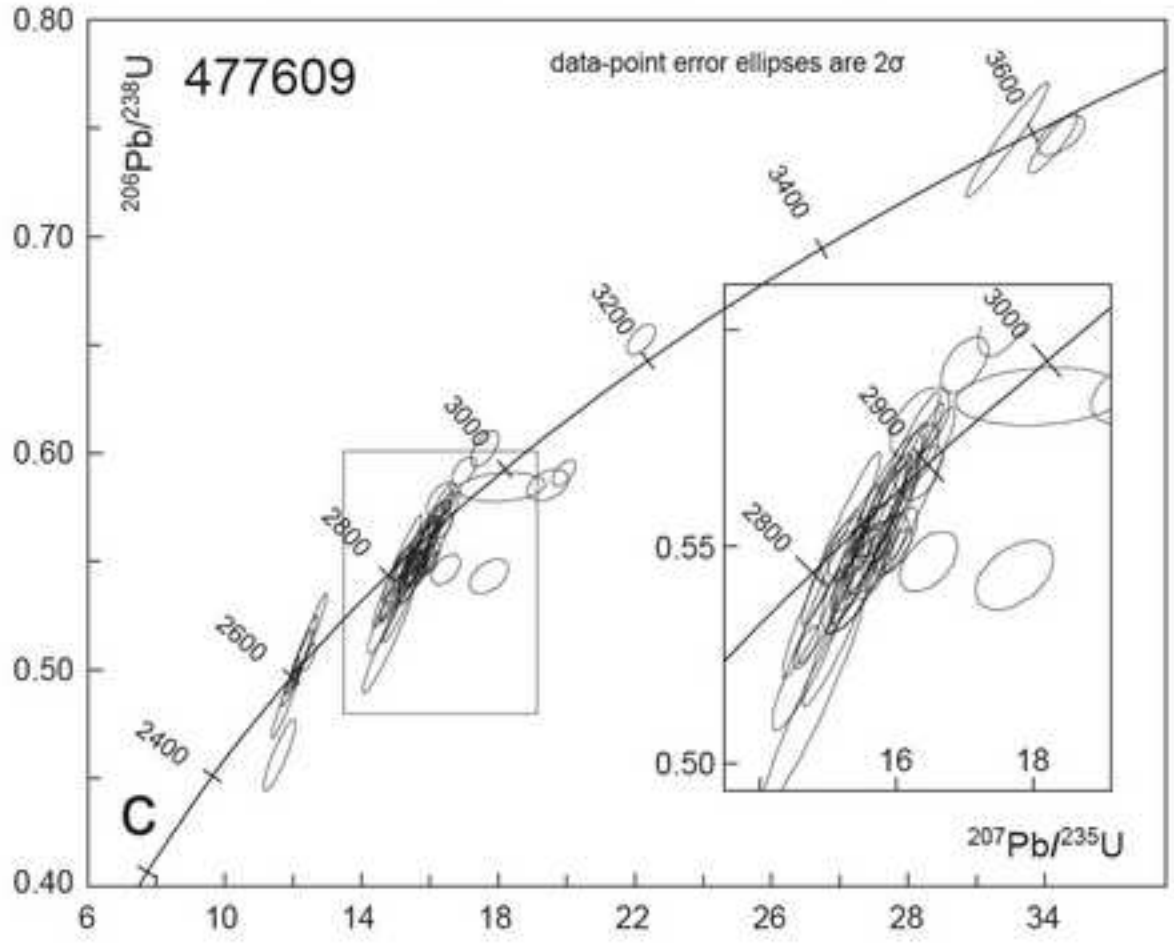

Figure 8

Click here to download high resolution image

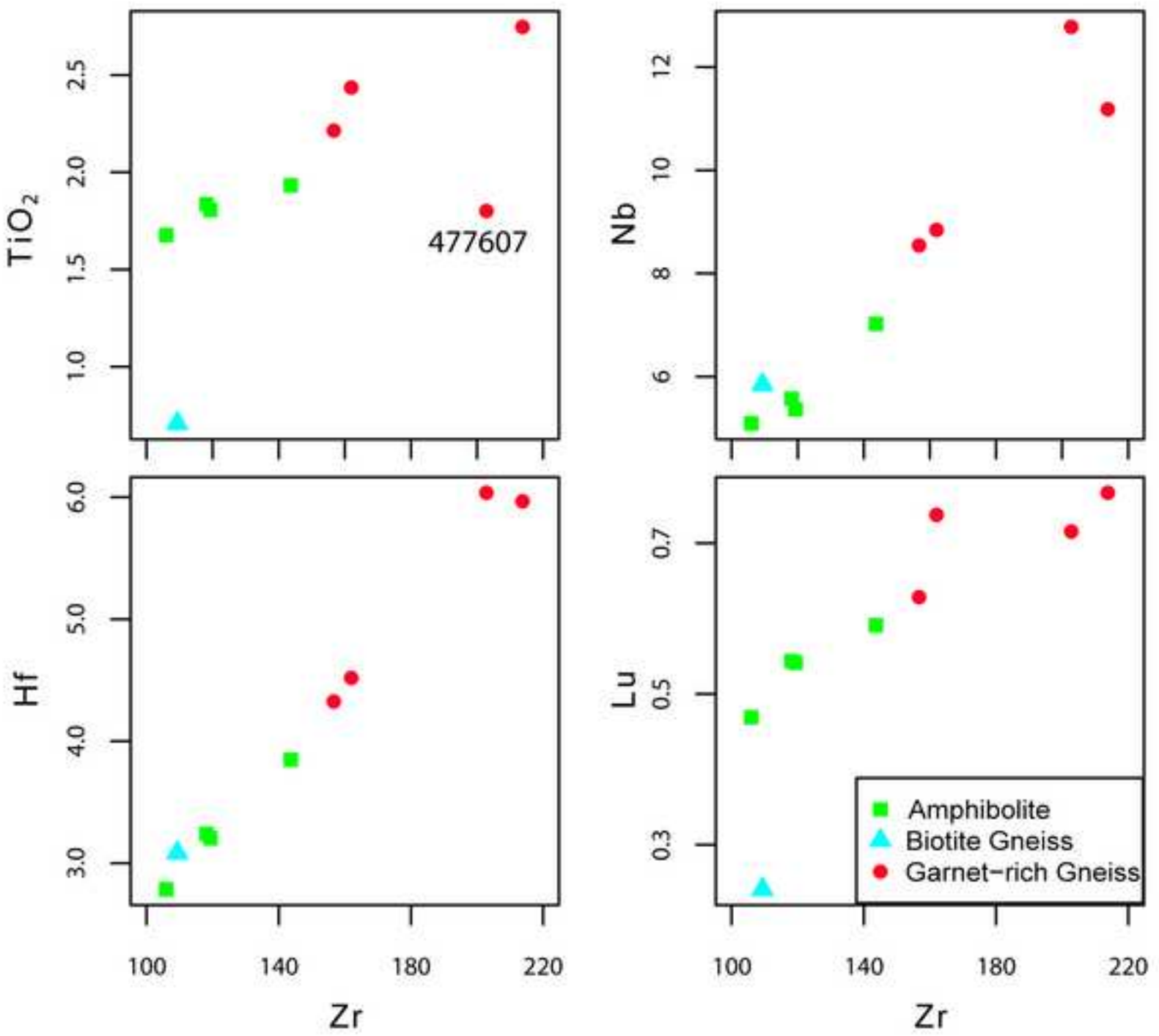

Figure 9

Click here to download high resolution image

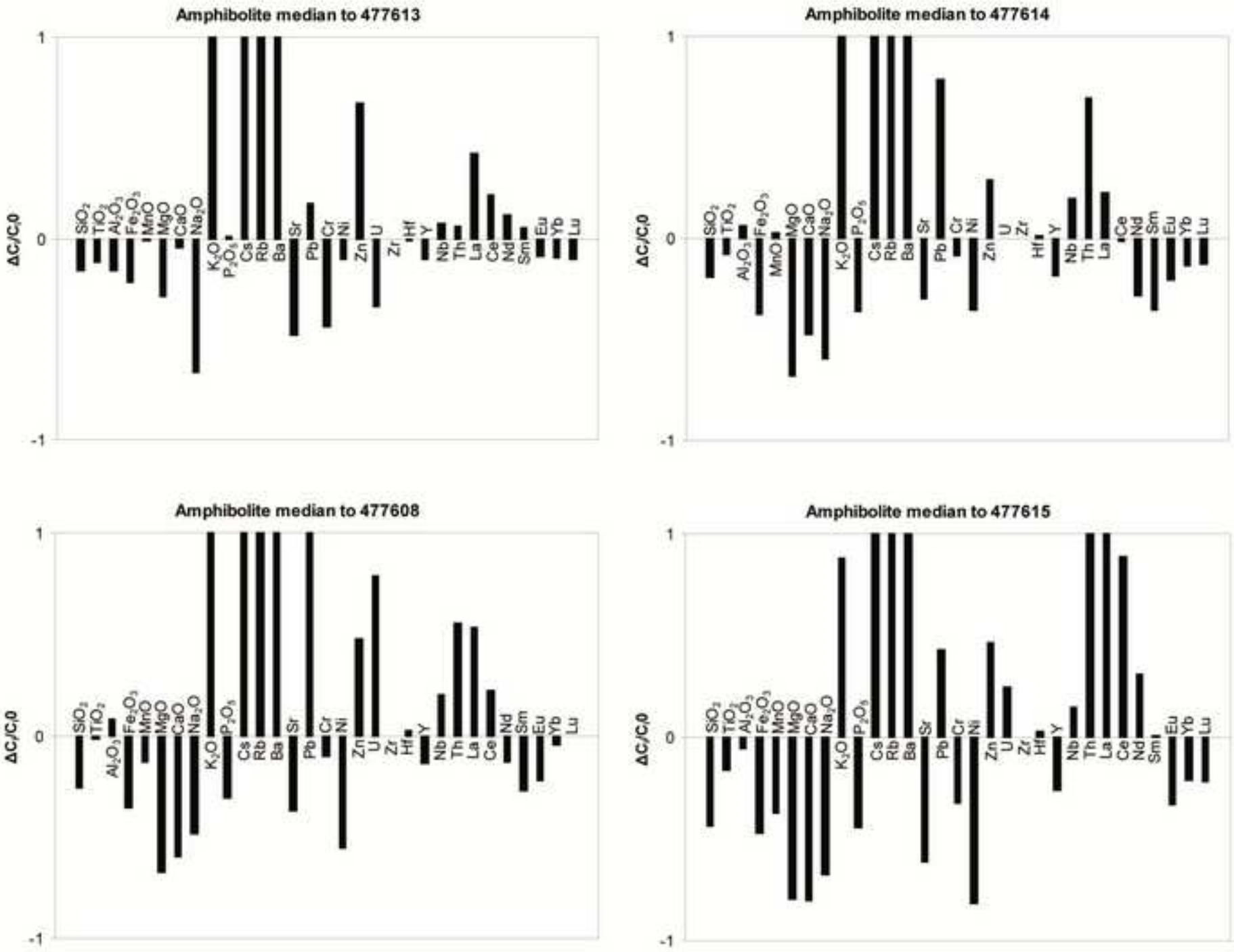

Figure 10

Click here to download high resolution image

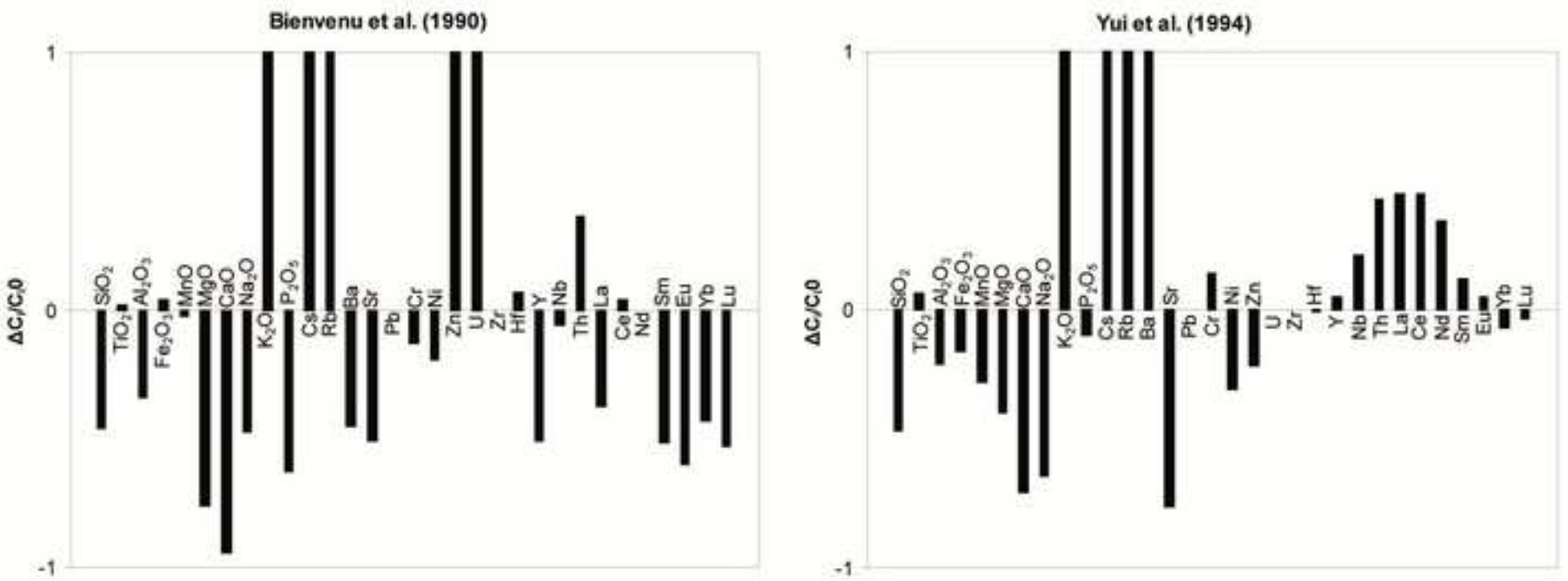

Figure 11

Click here to download high resolution image

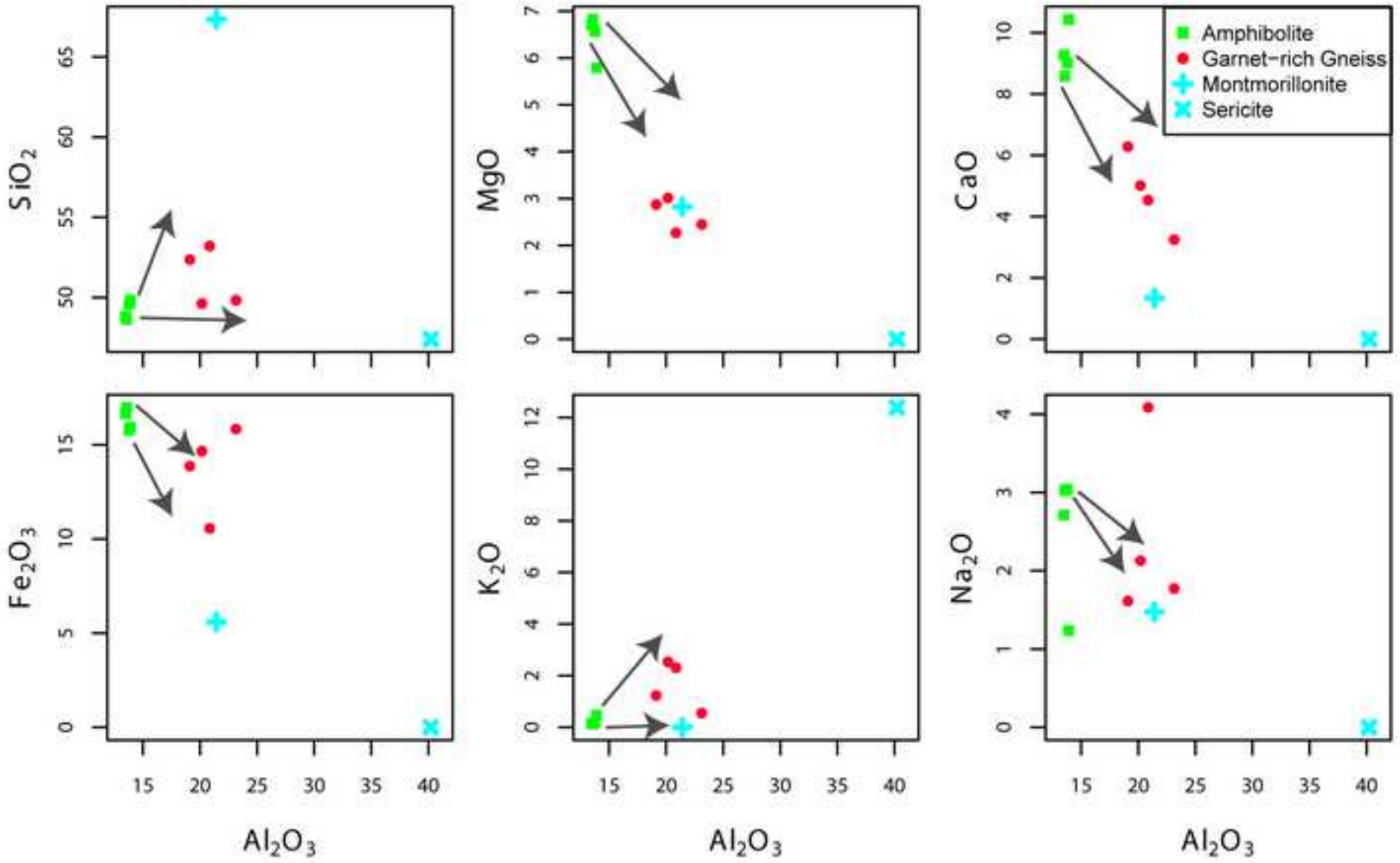

Figure 12

Click here to download high resolution image

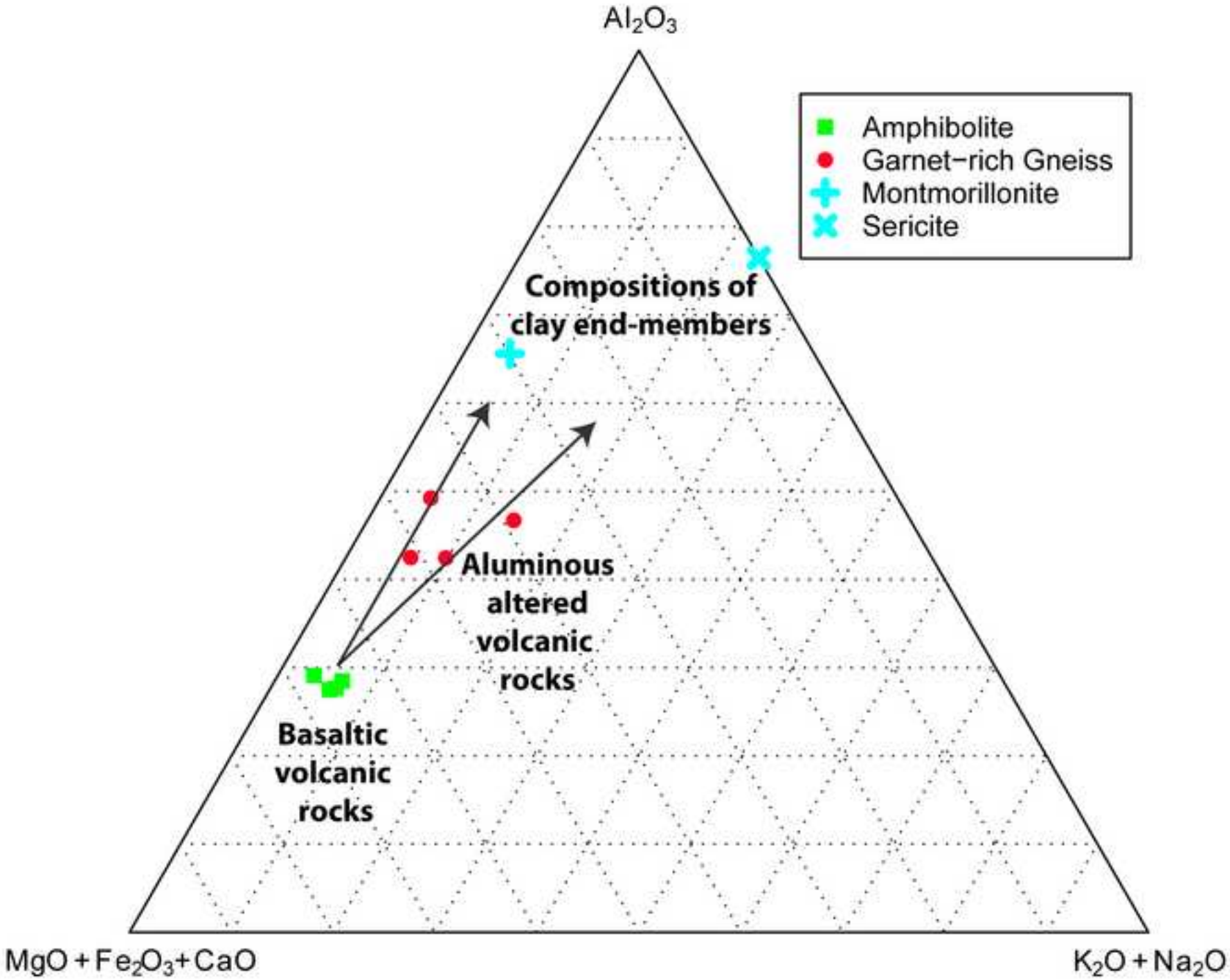

Table 1 Background dataset for online publication only

Click here to download Background dataset for online publication only: Table 1 - WR data.xls

Table 2 Background dataset for online publication only

Click here to download Background dataset for online publication only: Table 2 - Zircon U-Pb isotope data.xls

Table 3 Background dataset for online publication only

Click here to download Background dataset for online publication only: Table 3 Isocon results.xls